CANADIAN THESES ON MICROFICHE

I.S.B.N.

THESES CANADIENNES SUR MICROFICHE

National Library of Canada
Collections Development Branch

Canadian Theses on
Microfiche Service

Ottawa, Canada
K1A 0N4

Bibliothèque nationale du Canada
Direction du développement des collections

Service des thèses canadiennes
sur microfiche

NOTICE

The quality of this microfiche is heavily dependent upon the quality of the original thesis submitted for microfilming. Every effort has been made to ensure the highest quality of reproduction possible.

If pages are missing, contact the university which granted the degree.

Some pages may have indistinct print especially if the original pages were typed with a poor typewriter ribbon or if the university sent us a poor photocopy.

Previously copyrighted materials (journal articles, published tests, etc.) are not filmed.

Reproduction in full or in part of this film is governed by the Canadian Copyright Act, R.S.C. 1970, c. C-30. Please read the authorization forms which accompany this thesis.

THIS DISSERTATION
HAS BEEN MICROFILMED
EXACTLY AS RECEIVED

AVIS

La qualité de cette microfiche dépend grandement de la qualité de la thèse soumise au microfilmage. Nous avons tout fait pour assurer une qualité supérieure de reproduction.

S'il manque des pages, veuillez communiquer avec l'université qui a conféré le grade.

La qualité d'impression de certaines pages peut laisser à désirer, surtout si les pages originales ont été dactylographiées à l'aide d'un ruban usé ou si l'université nous a fait parvenir une photocopie de mauvaise qualité.

Les documents qui font déjà l'objet d'un droit d'auteur (articles de revue, examens publiés, etc.) ne sont pas microfilmés.

La reproduction, même partielle, de ce microfilm est soumise à la Loi canadienne sur le droit d'auteur, SRC 1970, c. C-30. Veuillez prendre connaissance des formules d'autorisation qui accompagnent cette thèse.

LA THÈSE A ÉTÉ
MICROFILMÉE TELLE QUE
NOUS L'AVONS REÇUE

NL-339 (r. 82/08)

Canada

0-315-08978-4

National Library of Canada | Bibliothèque nationale du Canada

91 Canadian Theses Division | Division des thèses canadiennes

Ottawa, Canada
K1A 0N4

56895

PERMISSION TO MICROFILM — AUTORISATION DE MICROFILMER

• Please print or type — Écrire en lettres moulées ou dactylographier

Full Name of Author — Nom complet de l'auteur

RONALD PATRICK PELOT

Date of Birth — Date de naissance	Country of Birth — Lieu de naissance
FEBRUARY 12, 1957	CANADA

Permanent Address — Résidence fixe

1055 WISEMAN CRESCENT
OTTAWA, ONTARIO
K1V 8J3

Title of Thesis — Titre de la thèse

FLOW CHARACTERISTICS IN THE AORTIC ARCH

University — Université

UNIVERSITY OF ALBERTA

Degree for which thesis was presented — Grade pour lequel cette thèse fut présentée

M.Sc

Year this degree conferred — Année d'obtention de ce grade	Name of Supervisor — Nom du directeur de thèse
1982	DR. C.M. RODKIEWICZ

Permission is hereby granted to the NATIONAL LIBRARY OF CANADA to microfilm this thesis and to lend or sell copies of the film.

The author reserves other publication rights, and neither the thesis nor extensive extracts from it may be printed or otherwise reproduced without the author's written permission.

L'autorisation est, par la présente, accordée à la BIBLIOTHÈQUE NATIONALE DU CANADA de microfilmer cette thèse et de prêter ou de vendre des exemplaires du film.

L'auteur se réserve les autres droits de publication; ni la thèse ni de longs extraits de celle-ci ne doivent être imprimés ou autrement reproduits sans l'autorisation écrite de l'auteur.

Date	Signature
January 12/82	Ronald Pelot

NL-91 (4/77)

THE UNIVERSITY OF ALBERTA

Flow Characteristics in the Aortic Arch

by

© Ron Pelot

A THESIS

SUBMITTED TO THE FACULTY OF GRADUATE STUDIES AND RESEARCH

IN PARTIAL FULFILMENT OF THE REQUIREMENTS FOR THE DEGREE

OF Master of Science

Mechanical Engineering

EDMONTON, ALBERTA

Spring, 1982

THE UNIVERSITY OF ALBERTA

RELEASE FORM

NAME OF AUTHOR Ron Pelot

TITLE OF THESIS Flow Characteristics in the Aortic Arch

DEGREE FOR WHICH THESIS WAS PRESENTED Master of Science

YEAR THIS DEGREE GRANTED Spring, 1982

Permission is hereby granted to THE UNIVERSITY OF ALBERTA LIBRARY to reproduce single copies of this thesis and to lend or sell such copies for private, scholarly or scientific research purposes only.

The author reserves other publication rights, and neither the thesis nor extensive extracts from it may be printed or otherwise reproduced without the author's written permission.

(SIGNED) Ronald Pelot

PERMANENT ADDRESS:

1055 Wisteman Cres.
Ottawa, Ontario
K1V 8J3

DATED December 17, 1981

THE UNIVERSITY OF ALBERTA

FACULTY OF GRADUATE STUDIES AND RESEARCH

The undersigned certify that they have read, and recommend to the Faculty of Graduate Studies and Research, for acceptance, a thesis entitled Flow Characteristics in the Aortic Arch submitted by Ron Pelot in partial fulfilment of the requirements for the degree of Master of Science.

C.A. Rodbard

Supervisor

D. Kennedy

M. Gardiner

Date December 17, 1981

Abstract

The flow patterns in a model of the aortic arch are studied by visualization under steady and pulsatile conditions. Particular attention is paid to secondary flow patterns, separation zones within the arch and flow distribution as a function of Reynolds number.

The flow is characterized by secondary flow vortices induced by centrifugal forces, a core of fluid which remains potential through the length of the arch and backflow areas along the inner curve wall and outer curve wall. The inner curve separation zone can be detected when the Reynolds number exceeds one thousand during steady flow, but persists throughout the period for pulsatile tests.

The sites of backflow coincide with the localization of atherogenesis and provide further evidence in establishing a correlation between hemodynamics and disease development in the aorta.

Acknowledgement

The author wishes to express his deep gratitude to Dr.Cz.M.Rodkiewicz who supervised this thesis. His expert guidance, continued encouragement and unending patience were greatly appreciated.

A special thanks to Karen Collinson for a major portion of the drafting and her moral support during my Master's program.

The companionship and assistance provided by my fellow student James Hildebrandt during the preparation of this thesis have been invaluable to me.

The author is grateful to the many office staff and technicians from the Department of Mechanical Engineering who provided assistance. Machinists Dennis Jessey and Bob Walker are particularly commended for their excellent work with the difficult arch models.

Financial support was provided by an N.S.E.R.C. post-graduate scholarship and research grant No.55-46221.

Finally, I would like to thank my family, whose encouragement was a great support to me, even while I was unable to be with them.

Table of Contents

Chapter	Page
1. Introduction	1
2. History of the problem	4
3. Background	9
4. Experimental Parameters	17
4.1 Geometric Parameters	17
4.1.1 Morphology	17
4.1.2 Aortic Dimensions	19
4.2 Flow Distribution	20
4.3 Fluid Properties	21
4.4 Flowrate	22
4.5 Velocity	23
4.6 Frequency and Waveform	24
4.7 Dimensionless Parameters	25
4.7.1 Reynolds Number	25
4.7.2 Parameters of Periodicity	26
5. Apparatus and Instrumentation	33
5.1 Flow Circuit	33
5.2 Model A	34
5.3 Model B	35
5.4 Piston	36
5.5 Cam	36
5.6 Pulsatile Flow Monitoring	37
5.7 Flow Visualization	38
6. Shear Stresses in Derivative Branches	48
6.1 Flow Partitioning	48

6.2 Factors Affecting Shear Stress 50
7. Separation Zones 58
7.1 Inner Wall Separation 59
7.2 Separation on the Outer Wall 63
7.3 Separation in Periodic Flow 65
8. Flow Patterns 77
9. Conclusions 94
References 96
Appendix I : Glossary 102
Appendix II : Non-dimensional parameters 105
Appendix III : Cam Design 108
Appendix IV : Injection Points 113
Appendix V : Inlet Section Design 117

List of Tables

Table	Page
4.1 Experimental Parameters	18
6.1 Pulsatile Shear Stress	52
IV.1 Dye Tap Locations	114

List of Figures

Figure	Page
1.1 Human heart and aorta	3
3.1 Sinus of Vasalva	13
3.2 Potential flow	14
3.3 Fully developed flow	14
3.4 Stresses induced by stagnation	15
3.5 Stresses induced by separation	16
4.1 Parts of the aorta	28
4.2 Branch flow distribution	29
4.3 Aortic arch twist	29
4.4 Aortic arch dimensions	30
4.5 Actual aortic pulsation	31
4.6 Design pulsation (Model B)	31
4.7 Sinusoidal simulation of heartbeat	32
5.1 Flow circuit	40
5.2 Experimental set-up	41
5.3 Model A	41
5.4 Fabrication of model A	42
5.5 Model A inlet section	42
5.6 Model B with and without twist	43
5.7 Model B rotatable sections	44
5.8 Model B inlet section	44
5.9 Pulsation apparatus	45
5.10 Dye pipe at inlet	46
5.11 Peripheral dye pipes	47

5.12 Dye reservoir bath 47
6.1 Flow distribution dependance on Reynolds number 54
6.2 Variation in distribution during cycle 55
6.3 Effect of α on wall shear stress 56
6.4 Effect of α on velocity profile 57
7.1 Separation in the brachiocephalic artery 67
7.2 Location of arch separation zones 67
7.3 Progression of inner wall backflow 68
7.4 Main flow bypassing inner wall separation 71
7.5 Three views of inner wall separation 72
7.6 Backflow along outer wall 73
7.7 Upper and lower vortices 74
7.8 Velocity profiles at several times 75
7.9a Filtered sinusoidal input 76
7.9b Actual unfiltered signal 76
8.1 Destination of inlet flow 86
8.2 Flow into the branches 87
8.3 Stagnation zones at branch inlets 88
8.4 Streamline in potential core 89
8.5 Dye injected into secondary flow vortex 90
8.6 Core streamline entering vortex 91
8.7 Trapped inner wall vortices 92
8.8 Dye streams twisting in inner wall vortex 93
III.1 Displacement curve 111
III.2 Cam and pitch profiles 112
IV.1 Coordinate system in arch 115
IV.2 Dye pipe numbering 116

List of Symbols

A	arch inlet area
β	screen porosity
c	radius of curvature of arch
d	screen wire diameter
D	arch inlet diameter
f	arbitrary function
L	arbitrary axial length
Le	dimensionless length parameter
p	static pressure
Q	flowrate
r	radial coordinate
R	arch inlet radius
Re	Reynolds number
s	general spatial coordinate
S	distance along centreline
t	time
T	period of oscillation
v	axial velocity
v'	peak velocity
$\bar{v}$	mean axial velocity
W	screen mesh spacing
z	axial coordinate
α	frequency parameter

List of Symbols

θ	azimuthal angle
λ	amplitude parameter
μ	dynamic viscosity
$\overline{\mu}$	average dynamic viscosity
ν	kinematic viscosity
ρ	density
$\overline{\rho}$	average density
σ	standard deviation
τ_w	wall shear stress
ϕ	degrees of arc
ω	angular frequency

1. Introduction

Much of the progress in medicine has come from exchanging acute medical problems for chronic ones. The increasing ability to understand, diagnose and cure diseases and defects has relegated many previously 'incurable' afflictions to the realm of improbability. The human cardiovascular system however remains a major cause of disability and death.

Engineering research in the field of hemodynamics (hydrodynamics of blood flow) provides information about the characteristics of blood flow through arteries and veins. Coupled with medical research, hemodynamics leads to a better understanding and possible correction of physiological impairments.

One such problem concerns the development of atherosclerosis in the arterial system. These lesions inhibit the flow and can ultimately block an artery to the point where the blood flowrate is critically low. There are several theories which have been proposed to explain lesion formation. Most of them have a biochemical basis but none comprise a complete explanation of this complex phenomenon.

The atherosclerotic lesions usually originate at specific sites in the large arteries, particularly at bends and branches. Therefore, hemodynamic theories have been advanced to relate lesion formation to the dynamic behaviour of blood at these sites. The aorta, an inverted U-shaped artery originating at the left ventricle (Fig.1.1) is of particular interest since it encompasses several potential lesion

sites.

A complete picture of the flow patterns in large arteries could provide clues to the cause and formation of atherosclerotic lesions.

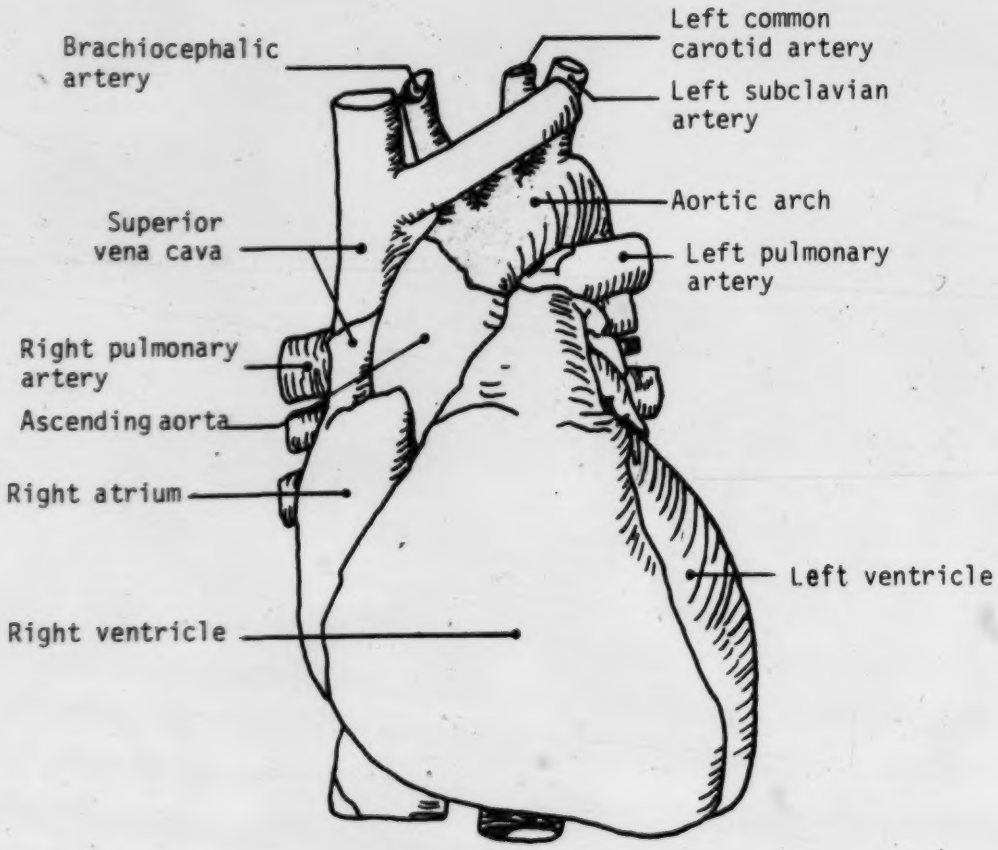

Figure 1.1 Human heart and aorta

2. History of the problem

The exact nature of the velocity distribution in the aorta plays an important role in the study of atherosclerotic formations. There are two major opposing theories which attempt to correlate primary atherosclerotic lesions with the dynamic behaviour of blood. Fry(1968) demonstrates a large increase in endothelial damage at high shear rates and subsequent deposition of blood elements at these locations. Conversely, Caro et al.(1971) contends that incipient atheroma (atherogenesis) coincides with low sanguinary shear rates which fail to adequately scour the arterial walls and prevent excessive plaque build-up. Scarton et al.(1976) postulates that one theory does not necessarily preclude the other, and that either effect may be the causal agent of atherogenesis at various sites.

The distribution of atherosclerotic lesions during the various stages of their development has been documented by several researchers. Some studies have been conducted on animals (ex. Rodkiewicz,1975), others on human cadavers (Shah et al.,1976) and some information about severe conditions has been gleaned by electrocardiographic and other diagnostic procedures (Rushmer,1970). Gresham(1976) presents an excellent review of experimentally induced and spontaneous atherosclerosis, particularly in primates.

Although many of the observations conflict, the affected areas in the aortic arch region generally include the inner curve of the arch and less severe formations on

the outer portion of the curve while the side walls are relatively unaffected. As well, there appears to be some build-up at the entrances of the large branches and on the proximal walls of these branches just beyond their inlet.

In light of these observations, a fluid flow investigation has taken place on several fronts. One approach consists of an analytical and/or numerical analysis making use of the Navier-Stokes equations with several simplifying assumptions. In its most basic form, the aortic arch can be modeled as a curved rigid tube. Dean(1927) considered this problem for steady laminar flow and demonstrated the nature of the secondary flow induced by centrifugal effects. The nature of pulsatile flow in circular straight pipes was examined by Womersley(1955a) and Uchida(1956). Unfortunately, the integration of these two analyses (Dean's and Womersley's) has defied rigorous and complete treatment due to its mathematical complexities. Smith(1975) has considered pulsatile flow in curved tubes, Chandran et al.(1974) analysed flow in curved elastic tubes and Singh(1974) looked at entry flow in a curved pipe. All of these mathematical treatments rely however on numerous simplifying assumptions including constant diameter, large curvature ratio and absence of branches. Curvature ratio is a non-dimensional parameter defined as the radius of curvature of a curved tube divided by the internal radius of the tube.

A second line of research involves direct measurement of velocity fields in an actual aortic arch. Studies of

blood flow in vivo have proven to be very difficult. The slow development of non-invasive probes had precluded most investigations on healthy humans, where the term healthy here denotes any person without significant heart diseases or defects. The time-varying contours of intravascular and intracardiac pressures have been easily measured externally and extensive investigations of these quantities have been accomplished by non-invasive techniques. By approximating arterial flow as pulsatile flow through infinite, rigid, circular tubes, Womersley(1955b) mathematically derived the velocity curve from the pressure measurement. However, the many simplifications inherent in applying such an analysis to the aorta prompted further developments in measuring the time-varying velocity more directly.

Several instruments were developed and improved over the years, initially focussing primarily on periarterial coupling. The electromagnetic flowmeter (Kolin,1936,1937), the pulsed ultrasonic flowmeter (Franklin,et al.,1959), the Doppler flowmeter (Franklin et al.,1961) and the hot-wire anemometer (Machella,1936; Ling et al.,1968) have all been considerably refined since their conception. These flowmeters have a common major drawback in that they require exposure of the artery. Therefore, their application has been limited to animals and to humans undergoing surgery. Although they provide an abundance of valuable information, these instruments again do not produce the velocity trace of a healthy human.

Miniature versions of these flowmeters and advances in surgical techniques have permitted the introduction of such devices into arteries by means of a catheter (Mills,1966; Mills and Shillingford,1967). The instantaneous velocity at various sites in healthy humans has thus been recorded by several researchers using intravascular probes (Gabe et al.,1969; Mills et al.,1970; Nichols et al.,1977a). However, these instruments initially could not measure spatial variation of velocity across the tube. Their application assumes uniform velocity across the lumen (McDonald,1974) and gives no indication of secondary flow patterns. This information is required for a complete mapping of the flow field.

Fortunately, further advances in instrumentation has stimulated more studies which yielded some velocity profiles in animal arteries. Seed and Wood(1970,1971) transversed the aortae of dogs with a hot-wire anemometer by directly puncturing the vessel wall. Farthing and Peronneau(1979) applied pulsed-Doppler ultrasonic transducers to the exterior of canine aortae which yielded velocity profiles at various sites and at different times throughout the cycle. Although the morphologies of the canine and human aortae are somewhat different, these results provide invaluable insights into the flow behaviour. Neither of these techniques can detect separation zones nor discern secondary flow patterns.

A final way to study the flow patterns involves the use of physical models. A drawback of this approach concerns the

limited degree of simulation obtainable in the laboratory, whether it be morphological reproduction, dynamic similarity or correspondence of various other characteristics. The great advantage of this method lies in the ability to control parameters at will and study their individual effects.

A number of researchers have considered the aortic arch flow from several points of view. For example, Rodkiewicz et al.(1976a) examined separation zones in a plastic model of the human aorta under steady and pulsatile flow conditions using hydrogen-bubble visualization. Austin and Seader(1973) experimentally studied the entry region of a curved tube while Scarton et al.(1976) revealed flow details in a curved glass tube. Since published results do not always agree due to differing experimental conditions, parameters and assumptions, this line of research continues until a single clear pattern emerges.

3. Background

A complete description of the aortic flow has not yet been formulated but several individual aspects have been revealed in various studies. Those characteristics which have been reasonably well established are reviewed in this section. Throughout this document, the terms *mean* and *average* are not used synonymously. They are respectively defined as:

$$f_{mean}\Big/_{s=cst} = \frac{1}{t_1}\int_0^{t_1} f(s,t)dt$$

$$f_{average}\Big/_{t=cst} = \frac{1}{s_1}\int_0^{s_1} f(s,t)ds \qquad (3.1)$$

where f is an arbitrary function of space(s) and time(t).

Modelling the aortic blood flow with a steady flowrate can be justified by several considerations. The pulsatile flow component is of the same order of magnitude as the mean forward flow. However, spatial variations in the wall shear stress depend primarily on the boundary layer growth due to the steady flow component. The fluctuating shear stresses caused by the oscillatory component are much less strongly dependant on position. Therefore, the mean shear stress has a spatial distribution similar to that of steady flow (Caro et al.,1971).

Likewise, Rodkiewicz et al.(1976a) has demonstrated that the locations of the separation regions can be similar for steady and pulsatile flow, notwithstanding their size

variation under fluctuating conditions. The similarity between the flattened velocity profile in the core of oscillatory flow (Atabek et al.,1964) and the flattened inlet velocity profile of steady flow further admits constant flow simulation. For these reasons, a steady flow model can demonstrate many characteristics of pulsatile flow.

Since the left ventricle acts as a reservoir and the aortic valve opens and closes very quickly, the velocity profile at the inlet to the ascending aorta is reasonably flat. This uniformity is further insured by the presence of the sinus of Vasalva, a deep narrow expansion of the aorta at the level of the coronary arteries which tends to absorb any jet effects during systole and also damps some vorticity originating at the valve (McDonald,1974) (Fig.3.1). This description has been supported by measurements in dogs by Seed and Wood(1971) and Farthing and Peronneau(1979) which show a remarkably flat profile in the ascending aorta.

As mentioned previously, flow in the aortic arch is similar in some respects to flow through a curved tube. In potential flow through a curved tube with a uniform velocity profile at the entrance, the total head $p+\frac{1}{2}\rho v^2$ remains constant along any streamlihe assuming the centreline lies in the horizontal plane. The static pressure increases with radius from the centre of curvature to balance the centrifugal force as the flow passes into the bend. Consequently the velocity increases at the inside of the bend while at the outer curve some velocity head $\frac{1}{2}\rho v^2$ is converted to

pressure head 'p' (Miller,1971). Coming out of the bend, the converse occurs to regain a uniform profile (Fig.3.2).

For fully developed flow of a real fluid entering a pipe bend, the slower moving fluid near the walls is acted on by a lower centrifugal force than faster moving fluid in the core. This central fluid is displaced outwards and the slow-moving boundary fluid moves inwards around the walls towards the inside of the bend describing a double helix (Fig.3.3). Dean(1927) theoretically analysed this problem for laminar flow while White(1929) experimentally investigated the flow behaviour as reviewed by Schlichting(1968).

Although the flow is much more complex for a real fluid, pressure differentials between the inside and outside walls differ little from those calculated assuming an ideal fluid. At the outlet from a bend, the flow on the inside experiences a pressure gradient of the same magnitude as that predicted for an ideal fluid. If sufficient velocity head is available to be converted to pressure head, the flow can negotiate the rise in pressure, otherwise it separates from the inner wall.

Since the fluid entering the aorta has a reasonably uniform velocity profile, the influence of curvature is less than in fully developed flow. This flow therefore does not fall into either of the above categories but rather exhibits characteristics of both. Theoretically, a potential core flow should persist through the length of the arch. The entry arc required for the flow to fully develop in a curved

tube as quoted by Scarton et al.,(1976) is given by:

$$\phi = 49 \left(\frac{R}{c}\right)^{1/2} Re^{1/3} \qquad (3.2)$$

where ø is degrees of arc measured from the entrance. For Re=1000 and (R/c)=3/4, fully developed flow would not be established until ø=424°. Since the aorta describes an arc of only 180° approximately, the flow is always developing.

Since the core remains potential, one would expect that the velocity at a cross-section varies inversely with the radius of curvature, which is supported by Farthing and Peronneau's(1979) measurements in dogs. However, the gradually developing flow will assume some characteristics of real fluid in curves and helices can thus form along the boundaries (Rodkiewicz et al.,1976a; Timm,1942).

Rodkiewicz(1976b) also gives evidence of separation and stagnation regions. Shear stresses act away from a stagnation arc (Fig.3.4a) which can deform the wall thus initiating a separation zone (Fig.3.4b). Conversely, shear stresses compress the wall lining towards a separation arc (Fig.3.5a) and as the wall loses resiliency a bulge may form thereby enlarging the separation region (Fig.3.5b). These two effects could intensify atherogenesis by particle circulation and deposition rather than removal and by damaging the protective biochemical defences of the wall cells (Fry,1968).

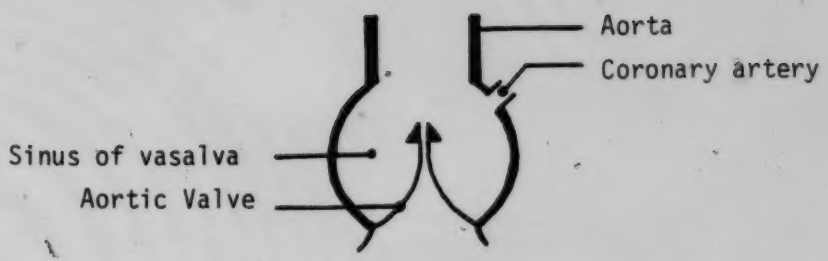

a.

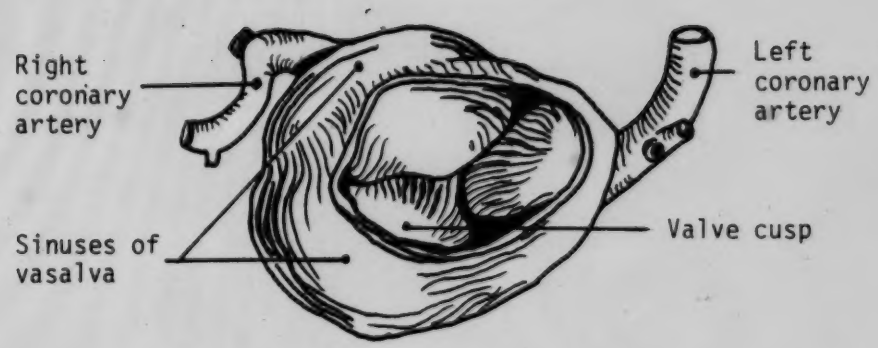

b.

Figure 3.1 Sinus of Vasalva

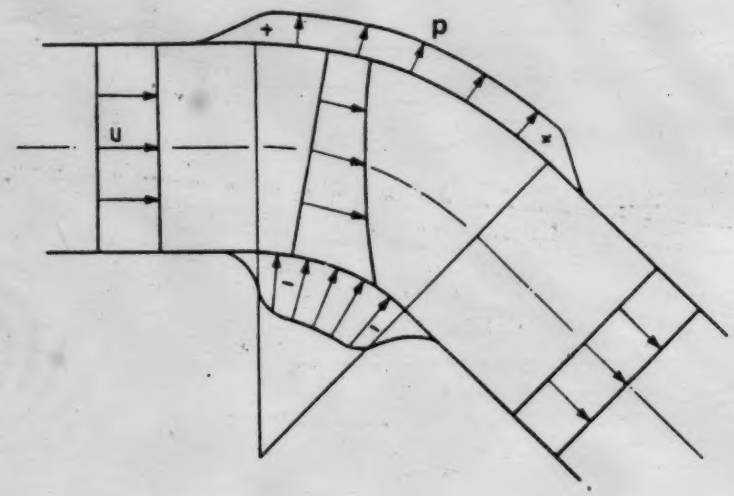

Figure 3.2 Potential flow

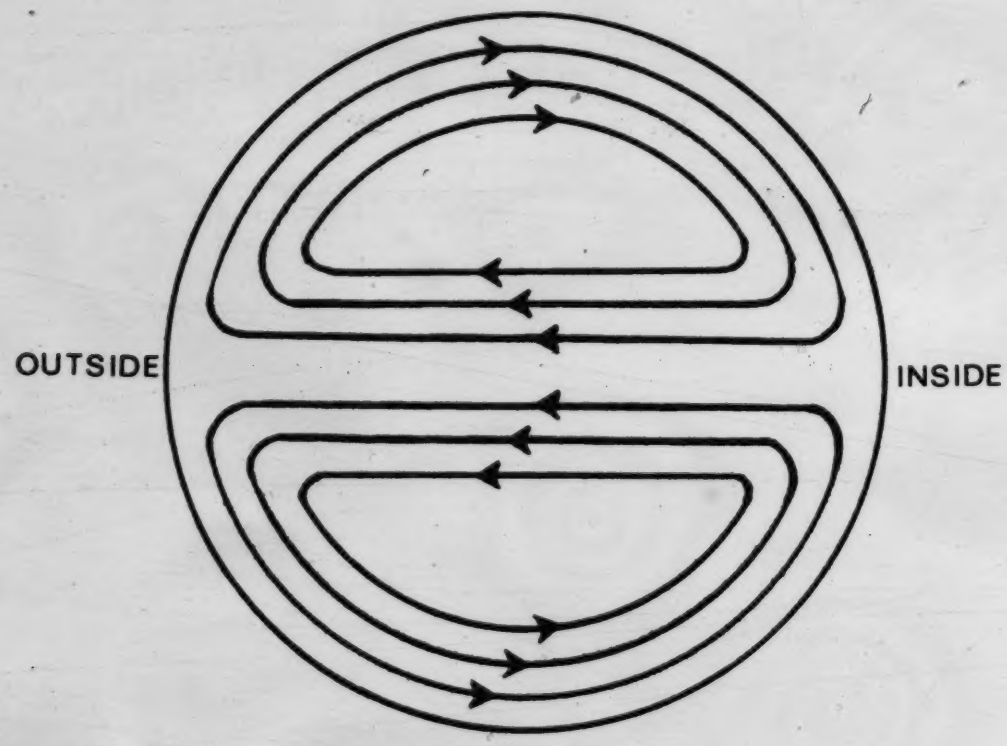

Figure 3.3 Fully developed flow(after McDonald, 1974)

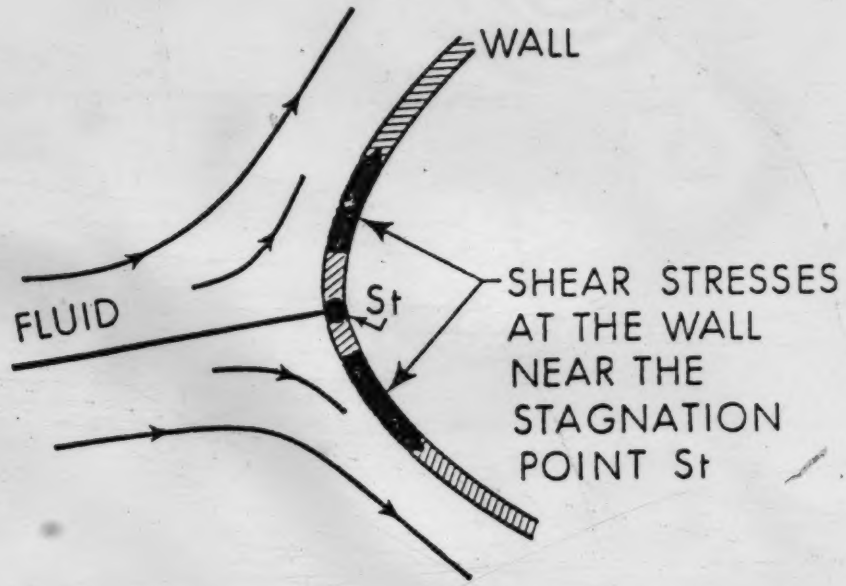

a.

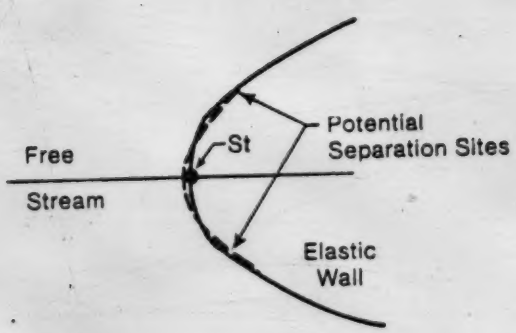

b.

Figure 3.4 Stresses induced by stagnation(Rodkiewicz,1980)

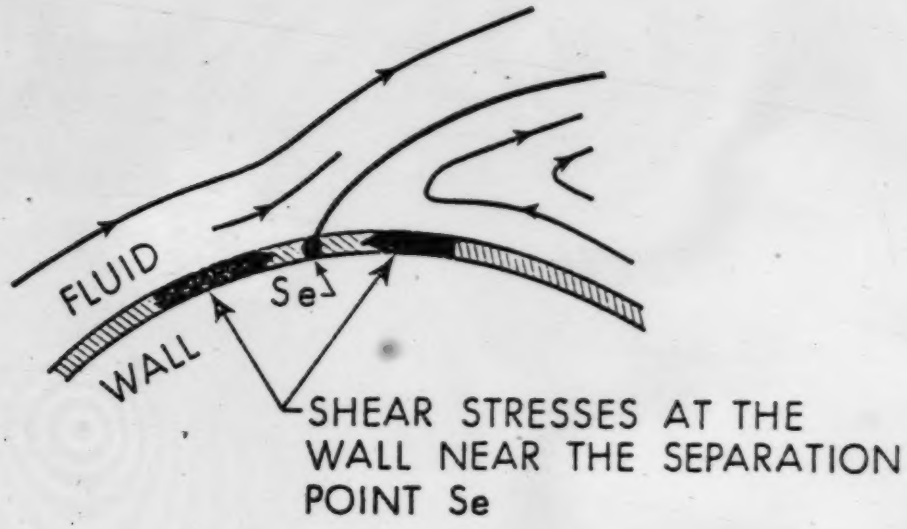

a.

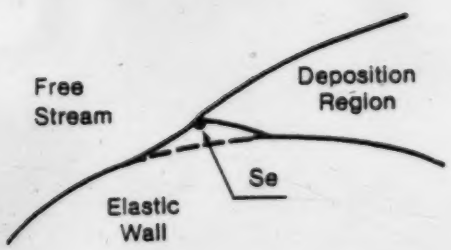

b.

Figure 3.5 Stresses induced by separation(Rodkiewicz,1980)

4. Experimental Parameters

From one individual to the next, there is evidently a great variation of the parameters which are related to flow in the aorta. However, a good starting point when dealing with experimental models is to set each parameter at the average value found in nature, and then in subsequent studies examine the effects of varying each parameter within its full physiological range. Unfortunately, large discrepancies in these parametric values are found in literature, therefore a comprehensive review is presented here. A summary of the average values used in this experiment as well as the normal physiological range is given in Table 4.1.

4.1 Geometric Parameters

4.1.1 Morphology

The aorta arises from the left ventricle of the heart, passes upwards (ascending aorta), bends over (aortic arch) then passes down through the thorax and abdomen (descending aorta), (Grant,1951) (Fig.4.1). The model in this study represents the aorta from the root to the proximal part of the descending aorta. The arch is characterized by continuous convergence and by three large branches originating at the top of the curve. There are two carotid arteries which supply most of the blood to the head and brain. The left and right subclavian each lead to an arm (or foreleg in the case

Table 4.1 Experimental Parameters

Parameter	Symbol	Average value	Normal range
Radius	R	1.45cm.	0.8-1.9cm.
Density	ρ	1.058g/cm^3	1.052-1.064g/cm^3
Dyn. visc.	μ	4.59cP.	4.11-5.07cP.
Kin. visc.	ν	4.34cSt.	3.88-4.79cSt.
Flowrate	Q	6 lit/min	3.5-7.5 lit/min
Velocity	v	15.1cm/sec	5.1-25cm/sec
Reynolds number	Re	1000	500-5000
Frequency parameter	α	18.8	10-30

of animals). The first branch from the aorta is the brachiocephalic artery which bifurcates into the right carotid and right subclavian arteries. For convenience, these branches and the descending aorta have been labelled 1A,1,2,3,4 and 5 respectively (Fig.4.2). The arch centerline does not lie completely in one plane but 'twists' backwards by approximately a 15° angle (Fig.4.3).

For this project, the coronary arteries are omitted since they are difficult to replicate faithfully and do not significantly affect the flow patterns in the arch. The ratio of their combined areas to that of the aortic inlet is less than 4% and together they consume only 3-4% of the blood flowing from the left ventricle. They originate at the sinus of Vasalva which almost completely damps any disturbing effects they might have on the downstream flow patterns. The twist is also neglected, hence the model centreline lies in one plane. The effect of twist on the flow pattern is left as another study.

4.1.2 Aortic Dimensions

The inside diameter at the base of the human aorta is largely underestimated in literature. An average value of 2.0-2.5cm. is often quoted and although this certainly falls within normal physiological range it is not representative of the mean. This discrepancy could arise from taking measurements from cadavers where the tissue has inevitably contracted or by estimations from X-ray photographs where

the boundaries are quite indistinct and magnification errors may occur.

Dotter and Steinberg(1949) angiocardiographically measured one hundred normal aortae and obtained a mean of 28.6mm. with a range of 16-38mm. for the inside diameter at the mid-ascending aorta. Furukawa et al.(1976) found similar values from echocardiograms of 194 normal aortae. Their measurements yielded a mean internal diameter of the aortic root at the end of diastole of 28mm. with a range of 14-39mm.

Since the present model originates between the aortic root and the mid-ascending aorta, and since the diameter is 2-3% larger during systole, a value of 29mm. has been adopted as a suitable average.

The dimensions of the aortic arch and its derivative branches are shown in Figure 4.4. The data have been culled from several sources (Reich,1949; Meschan,1975; Reul et al.,1974; Rodkiewicz et al,1979) due to a lack of agreement on average values and absence of a single comprehensive review.

4.2 Flow Distribution

The volumetric distribution of the flow in each branch is an important factor in the replication of the actual flow patterns. According to Reul et al.(1974), about 4% of the inlet flow to the ascending aorta flows through each

subclavian artery, while approximately 7% is diverted through each carotid artery leaving 78% to continue its course through the descending aorta. This agrees with values cited in Guyton(1956) and Ruch and Patton(1973) although these sources do not provide a complete list. The model in this experiment has therefore been calibrated to the appropriate distribution(Fig.4.2).

4.3 Fluid Properties

The dynamic viscosity of blood has been one of the most critically and comprehensively studied blood flow parameters (ex.Chien,1979). Blood is essentially a viscoelastic fluid and at a given temperature the fundamental factors affecting its viscosity are cell concentration, plasma viscosity, cell deformation and cell aggregation. However, for a given hematocrit (% cells in plasma), at shear rates between 10^2-10^3 sec^{-1}, in tubes with internal diameter greater than 1mm., the viscosity becomes virtually constant (McDonald,1974; Haynes,1961; Bayliss,1962). The lower limit on tube size is required since tests have shown that as the ratio of blood cell diameter to tube diameter becomes small the viscosity tends towards a constant value, all other things being equal. Since the aorta satisfies the stipulated criteria and hematocrit varies little between healthy individuals, it is possible to assume a constant viscosity thereby allowing the use of any Newtonian fluid (such as water) as the working

medium.

Rosenblatt(1965) quotes a mean viscosity $\bar{\mu}$ =4.59cP. at body temperature (37°C) with a standard deviation of σ =.485 for 117 normal male adults studied. The average value for females is about 14% lower but since the occurence of severe atherosclerosis predominantly affects men, this study will adopt values representative of adult males, ergo $\bar{\mu}$ =4.6cP.

In comparison, blood density has a much smaller physiological range and is much more amenable to accurate measurement. Most sources (Muirhead et al.,1946; Gray and Elliot,1943) concur on an average blood density of $\bar{\rho}$=1.058g/cm³ with a limited range $1.052 \leq \rho \leq 1.064$ g/cm³.

A proper evaluation of these fluid properties is critical to ensure dynamic similarity of the actual aorta and the model (Section 4.8).

4.4 Flowrate

The variability of the average flowrate in normal physiological situations exceeds that of all the other relevant parameters. Eclipsing the normal variation from one individual to another, the large range is primarily a function of activity level as well as sex, physical size, age and other minor factors (Detweiler,1972). Although the range extends from 3.5 litres/min. for a small adult woman at rest to 45 litres/min. for a well-conditioned athlete engaged in vigorous exercise, one may assume that only a small range is

applicable to the study of atherosclerosis. Since middle-aged men and elderly people are most susceptible to the debilitating effects induced by advanced atheroma, and many have a low level of physical activity, a value of 6 litres/min. is deemed representative of resting, sitting and light walking conditions (Guyton, 1956; Bergel, 1972) and a range from 4-8 litres/min. would encompass a large percentage of normal subjects. The accuracy of this assumption is not critical however since the overall flow field should not be affected significantly by this parameter.

4.5 Velocity

Values of velocity in the aorta found in literature are difficult to compare since they are alternately given as peak value, mean systolic or mean velocity. They are also estimated at various cross-sections in the aorta and a uniform velocity profile is usually assumed at the site in question. The most consistent and expedient approach is to calculate the mean velocity from the flowrate and ascending aorta dimensions:

$$\bar{v} = \frac{Q}{A} = \frac{6.0\ \text{L/min}}{\pi(1.45)^2\text{cm}^2} = 15.1\ \text{cm/sec} \qquad (4.1)$$

This estimate falls somewhat below commonly quoted values (Detweiler, 1972 ; Prec, 1949). The discrepancy can be attributed to measurements at sites other than the aortic

root and/or higher flowrates than the sedentary 6 litres/min.

4.6 Frequency and Waveform

The frequency of the pulsations depends on the same parameters as the flowrate (sec.4.4). The resting rate can be as low as 50 beats/min. for a well-conditioned person (McDonald,1974) and peak at 270 beats/min. during short exhaustive work (Guyton,1956). An average value for an adult refraining from strenuous activities can be assumed at about 70 beats/min. (Best and Taylor,1952; Altman and Dittmer,1971). The velocity waveform in the arterial system has been extensively analysed. As mentioned in Section 2., reliable velocity waveforms can now be measured in the aortae of healthy people. Several publications compare graphs of normal and deviant velocity waveforms. For simulation, a waveform which appears representative of the norm has been selected from a paper by Nichols et al.(1977b) (Fig.4.5).

The pulsation is characterized by a sharp peak during systole followed by a small backflow period and then minor oscillations during diastole. In the ascending aorta, the flow reversal does not occur to any significant extent (McDonald,1974) and the minor oscillations are largely due to the elastic properties of the vessel wall rather than backflow through the valve. Therefore, for experimental simplicity, zero flow is assumed for the complete diastole

period (Fig.4.6). The effects of this approximation would require further study.

4.7 Dimensionless Parameters

The model need not be identical to the actual aortic arch to yield a correct flow analysis. Provided that certain relationships of the relevant parameters are maintained, the flow behaviour in the model corresponds to the physiological situation. These relationships between certain dynamic and kinematic flow characteristics are represented by dimensionless parameters.

4.7.1 Reynolds Number

For flow through a geometrically similar model of the aortic arch, dynamic similarity is achieved only when the Reynolds number, Re, (Appendix II) is the same at every point in the flow at every instant in time. In other words, if the inlet conditions are identical in the model and actual aorta, setting the Re the same at two geometrically corresponding points ensures dynamic similarity of the flow everywhere in the prototype (within the previous constraints of inelasticity, no twist, etc). Since this experiment assumes uniform velocity profile at the entrance (Section 3.), it is sufficient to assume the appropriate Re based on the instantaneous average velocity at the inlet of the aorta.

In the case of steady flow, dynamic similarity is therefore achieved by adjusting the flowrate to yield a Reynolds number within physiological range. A Re of 1000 corresponds to the net positive flow in the aortic arch (ie.cardiac output)(Appendix II). At peak systole, Re attains a value circa 5000, which would be reflected in the model by a higher flowrate.

4.7.2 Parameters of Periodicity

For pulsating flow, it is not sufficient to use a Re based on time-averaged flowrate since the frequency, amplitude and shape of the velocity waveform play an important role in the fluid behaviour.

The unsteadiness parameter α is a non-dimensional quantity which characterizes kinematic similarities in the liquid motion. A typical value based on the experimental parameters selected earlier is $\alpha=19$ (Appendix II). McDonald(1974) quotes a range of $13.5 \leq \alpha \leq 16.7$ at the aortic root based on a pulse of 55-72 beats/min. and a radius of 1.08-1.11cm. As discussed earlier, this radius estimate is low. Recalculating these limits using R=1.45cm. yields $17.6 \leq \alpha \leq 22.4$ which concurs with the value chosen above.

Having specified a parameter accounting for frequency similarity, it remains to define the amplitude of the waveform. Decomposing the periodic flow in the cardiovascular system by a Fourier series, it has been shown that the first harmonic predominates (McDonald,1974). Therefore one form

previously adopted has been to approximate the fluctuations by a sinusoid of a certain amplitude superimposed on a mean forward flow (ex. Rodkiewicz et al.,1976a). This type of waveform is formulated by:

$$\lambda = \frac{v_{max} - v_{min}}{\bar{v}} \qquad (4.2)$$

where λ , the amplitude parameter, has previously been studied in the range $0 \leq \lambda \leq 2$ with the lower value representing steady flow and the higher value approaching an actual waveform (Fig.4.7). This method does not take into account the fact that the systole's duration is only 1/3 of the total period, and that a zero flow stage is required to simulate diastole. However, the great advantage of this approach lies in its generality and ease of reproducibility.

The experiments reported here use either steady or sinusoidal flow. However, the design of a more advanced model (Section 5.3) adopts a characteristic velocity curve (Fig.4.6) and the corresponding cam profile produces the same waveform with minor modifications (Appendix III). This method allows comparisons with sinusoidal pulsations and should the differences be insignificant, the latter could be adopted without reservations.

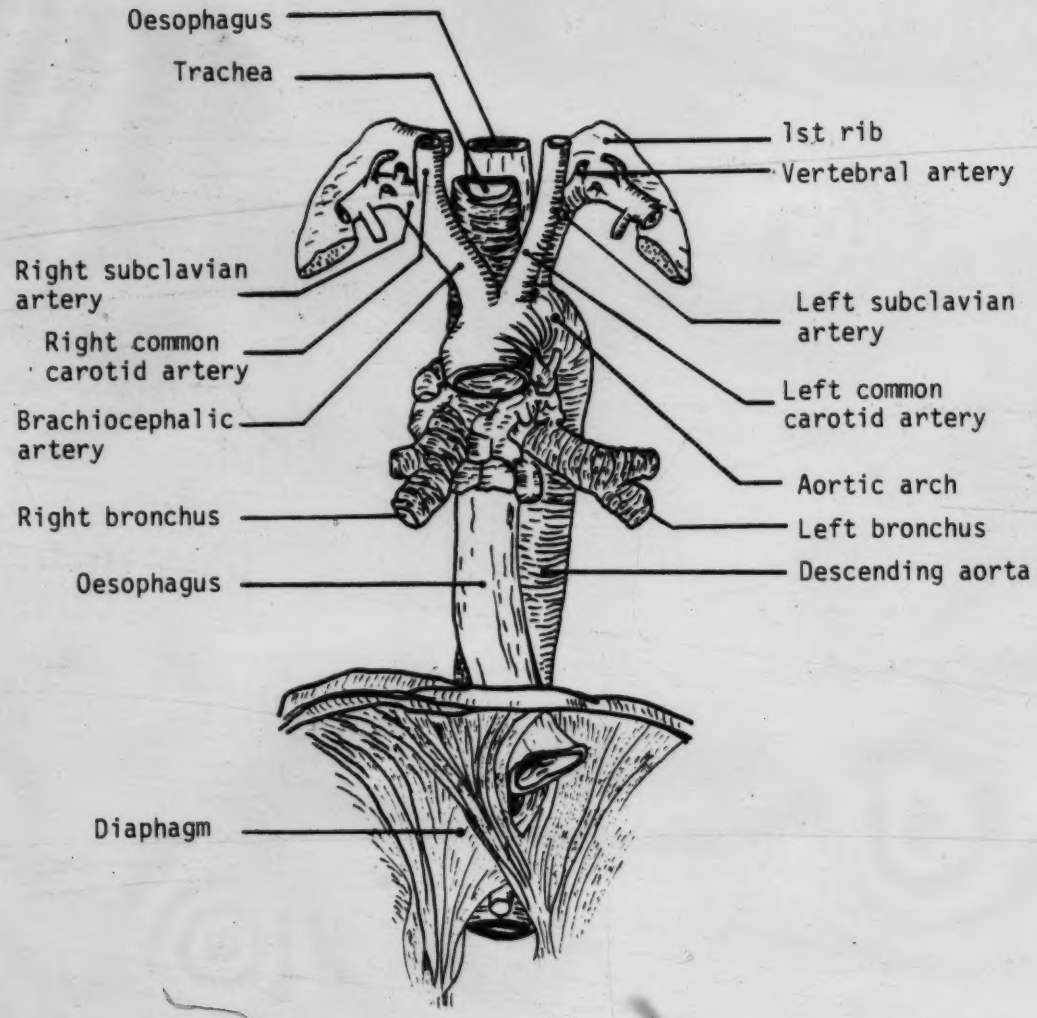

Figure 4.1 Parts of the aorta

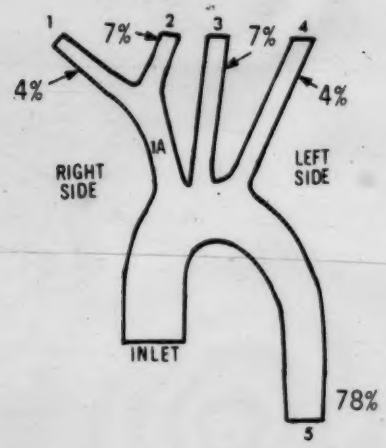

Figure 4.2 Branch flow distribution

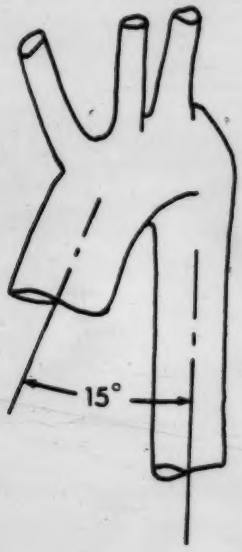

Figure 4.3 Aortic arch twist

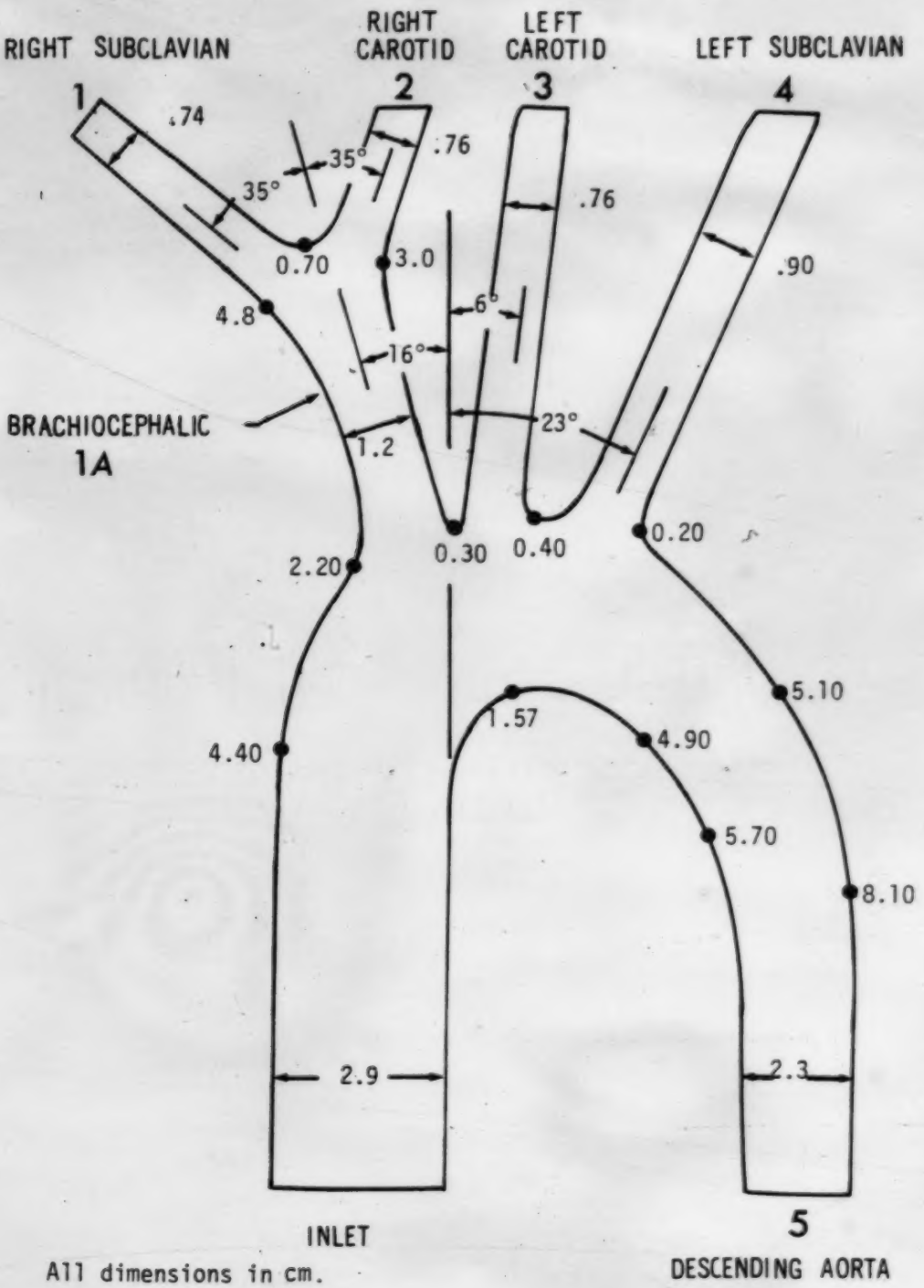

Figure 4.4 Aortic arch dimensions

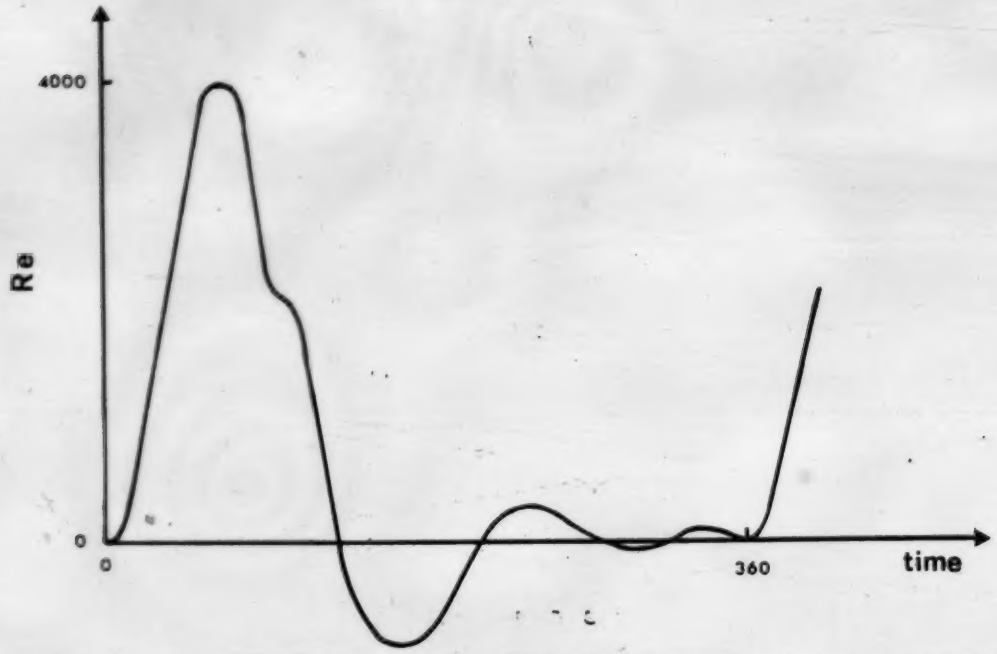

Figure 4.5 Actual aortic pulsation(after Nichols,1977b)

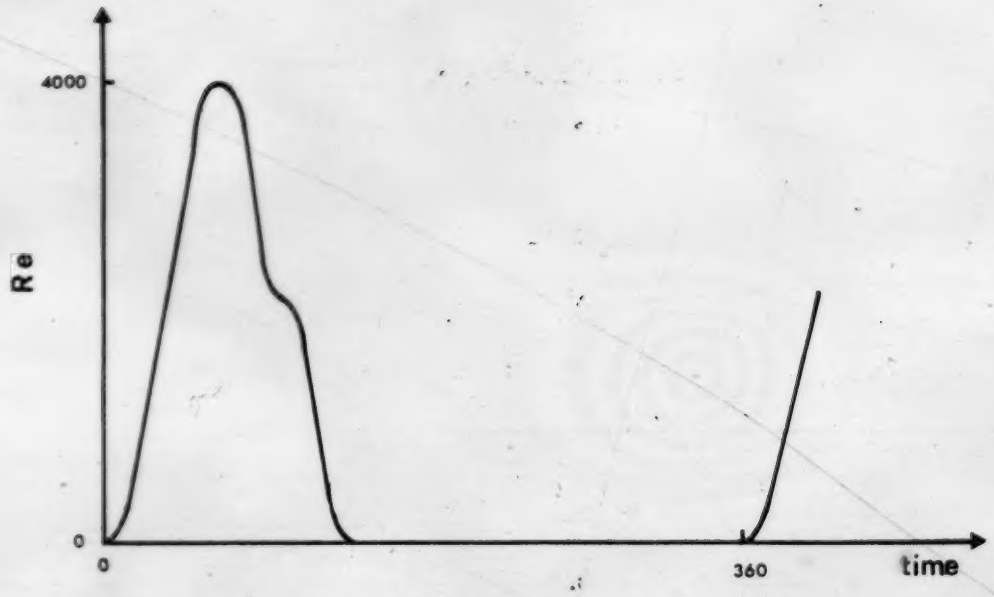

Figure 4.6 Design pulsation (Model B)

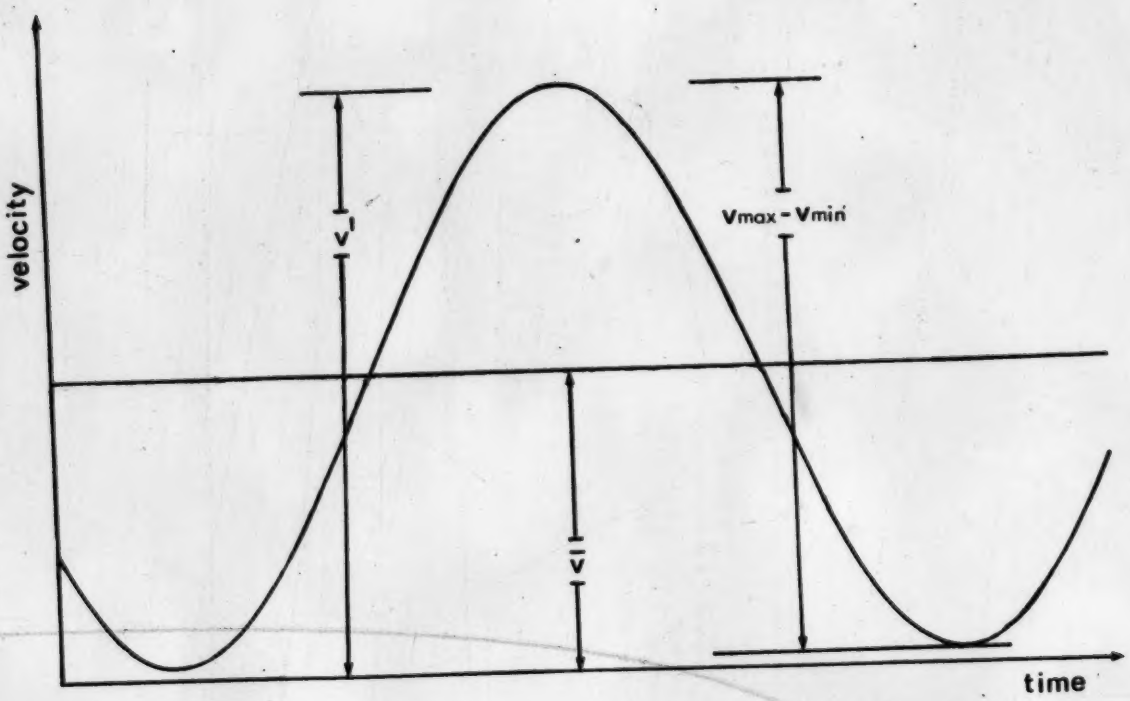

Figure 4.7. Sinusoidal Simulation of Heartbeat

5. Apparatus and Instrumentation

As discussed in Section 4, several simplifying assumptions were required to produce a feasible model. All of the tests carried out in this experiment make use of one model, *A*, which includes some characteristics of an actual aortic arch. Concurrently, a second model, *B*, was designed to incorporate several improvements over model *A* and serve for future experiments. These models are described in detail in the following sections.

5.1 Flow Circuit

The flow circuit for each of the two models is fundamentally the same. A schematic and picture of the flow circuit are shown in Figures 5.1 & 5.2. The working fluid must be replaced periodically as the dye used for visualization eventually darkens the water. To replace the fluid, fresh tap water is settled in an auxiliary reservoir for a period of several hours to prevent air bubbles from settling out in the model.

A rotameter is used to roughly set the total flowrate in the model. The distribution of the flow to the branches varies with the total flowrate through the model (Section 6.). To maintain a distribution within the physiological range, a flow restrictor on each branch must be adjusted as a function of total flowrate. Orifice plates are used on model *A* while conic valves are installed on model *B*.

To monitor the flowrate in each branch, individual collection tanks labelled T1 to T5 are used in conjunction with a stopwatch. These tanks in turn drain into a common reservoir which feeds the pump to complete the circuit.

The surge tank, partially filled with water, acts as a buffer for pump fluctuations and traps air bubbles generated upstream. The piston apparatus is an optional attachment to superimpose regular pulsations on the steady pump flow. Finally, a 20 foot long straight section, exceeding the entrance length required to attain fully developed flow at maximum physiological Reynolds number, ensures that the flow conditions upstream of the model are known and consistent.

5.2 Model A

This model is scaled to three times actual size and its centreline lies in one plane (Fig.5.3). It was fabricated by machining two slabs of acrylic and then gluing the two symmetrical halves together (Fig.5.4). The outlet sections are all positioned at the same level, about two inches above the model centreline. The flow distribution is controlled by a removable orifice plate in each outlet section.

The inlet section (Fig.5.5) consists of an enlarged section with a transverse screen to flatten the velocity profile. The slightly flared model inlet then captures the core flow thus producing a uniform velocity profile with a very thin boundary layer at the entrance to the arch.

5.3 Model B

This model was built to incorporate several improvements over model *A*. The principal alteration was to allow for the 15° twist of the arch (Fig.5.6). This was achieved by splitting the model into five separate sections each of which can be rotated about the model centreline at the interfaces of sections (Fig.5.7). Hence the model can assume any angle of twist in the range of about -10° to 30°. To achieve this capability however, visualization had to be compromised.

Several design modifications were made to the inlet section of this model as well (Fig.5.8). To better assure a uniform velocity profile at the entrance to the arch, the following design factors were considered:

a. four successive screens will cause a thorough transfer of momentum across the inlet section to produce a uniform velocity profile (Appendix V).
b. a bell-shaped entrance is provided at the arch inlet to inhibit flow disturbances.
c. fluid is bled from the inlet section behind the bell-shaped entrance to streamline the flow and prevent vortices from forming.

5.4 Piston

The piston is cam-driven by a 2-Hp DC variable speed motor (Fig.5.9). The piston superposes fluctuations on the steady flow supplied by the pump. Since the oscillation apparatus was appropriated from a previous experimental set-up, the cam design required retrofitting to the existing apparatus. In other words, the fixed bore and limited stroke of the cylinder impose constraints on the cam design.

5.5 Cam

The velocity profile shown in Figure 4.6 is a simplification of an actual human pulsation. The backflow period and minor diastolic oscillations are neglected to simplify the cam design. It is postulated that this change would not significantly affect most aspects of the flow in the model.

Initial attempts to design a cam based on the approximate profile yielded a pressure angle in the order of 50°-60°. Since it was found that a feasible cam profile could not be easily produced, a computer subroutine was written to produce the appropriate cam outline from input data containing the desired displacement curve, base circle radius, amount of offset and follower radius (Appendix III). This subprogram would calculate the maximum pressure angle for a given profile and plot the resulting contour.

A sinusoidal pulsation was applied to model *A* to examine its effects on the separation zones. The cam was

designed using λ =1.9 and an average Re of 1000.

For eventual use on model *B*, a cam was designed which would produce the waveform shown in Figure 4.6. This could lead to studies on the effect of waveform on various flow phenomena in the arch. The computer program would facilitate the production of various other waveforms as well.

5.6 Pulsatile Flow Monitoring

An Annubar flowmeter was installed in the pulsatile flow circuit to monitor the fluctuating flow and ensure that the imposed oscillations are producing the desired result. The Annubar, a device using a calibrated Pitot tube arrangement which yields an output proportional to the flowrate, is connected to a DP45 Validyne pressure transducer. This signal is picked up by carrier-demodulator and transmitted to a oscilloscope. A low-pass filter suppresses unwanted frequencies from the signal.

The Annubar is specifically designed for steady flow but was deemed sufficiently accurate for the extremely low frequencies of fluctuations used in this test. However, for a better response, particularly at the higher frequency required for model *B*, an electromagnetic flowmeter is recommended. Some of the instruments discussed in Section 2. can be adapted to detect flow direction, which is advantageous for actual waveform simulation.

5.7 Flow Visualization

The flow patterns are visualized by injecting a fine stream of dye through 0.5mm I.D.tubing. The dye was alternatively introduced at various positions at the entrance to the arch or points along the aortic walls. At the inlet, the dye pipe is fixed in a ring which permits angular positioning for 180° range and transverse adjustment completely across the lumen (Fig.5.10). Figure 5.11 indicates some peripheral injection points along the inner curve wall and on the top of the model. The exact non-dimensionalized locations of these wall taps are given in Appendix IV.

It is very important to maintain the densities of the dye and working fluid as close as possible to each other. Since the pump causes a temperature rise of about 6°C over a two-hour period of continuous operation, the water density continuously decreases. To compensate for this effect, the dye reservoir is submersed in a water bath which is fed from the working fluid (Fig.5.12). It is advantageous to maintain a constant dye velocity to provide stable conditions during visualization. By using a reservoir with a large diameter relative to that of the dye pipe, the loss of head in time becomes negligible. At the entrance to the model, the dye is injected with about the same momentum as the inlet flow. At the wall taps the dye is injected with the lowest possible momentum which still allows adequate visualization.

The photographs were taken with a Canon F-1 camera using a 55mm lens, and optional 240mm and 450mm close-up

lenses, either individually or superimposed. Lighting was provided by one or two 200 watt tungsten lamps placed under the model. A single sheet of mylar was also placed between the lamps and the model to further diffuse the light and provide more uniform illumination. The black and white photographs of the flow were taken with 400 ASA tungsten Tri-PanX and the colour pictures using 400 ASA Ektachrome. Although perhaps not intuitively obvious, the visual distortion inherent in the model due to the curved inner walls and flat outer surface is less than if the outer surface were also curved (Roussel, 1971).

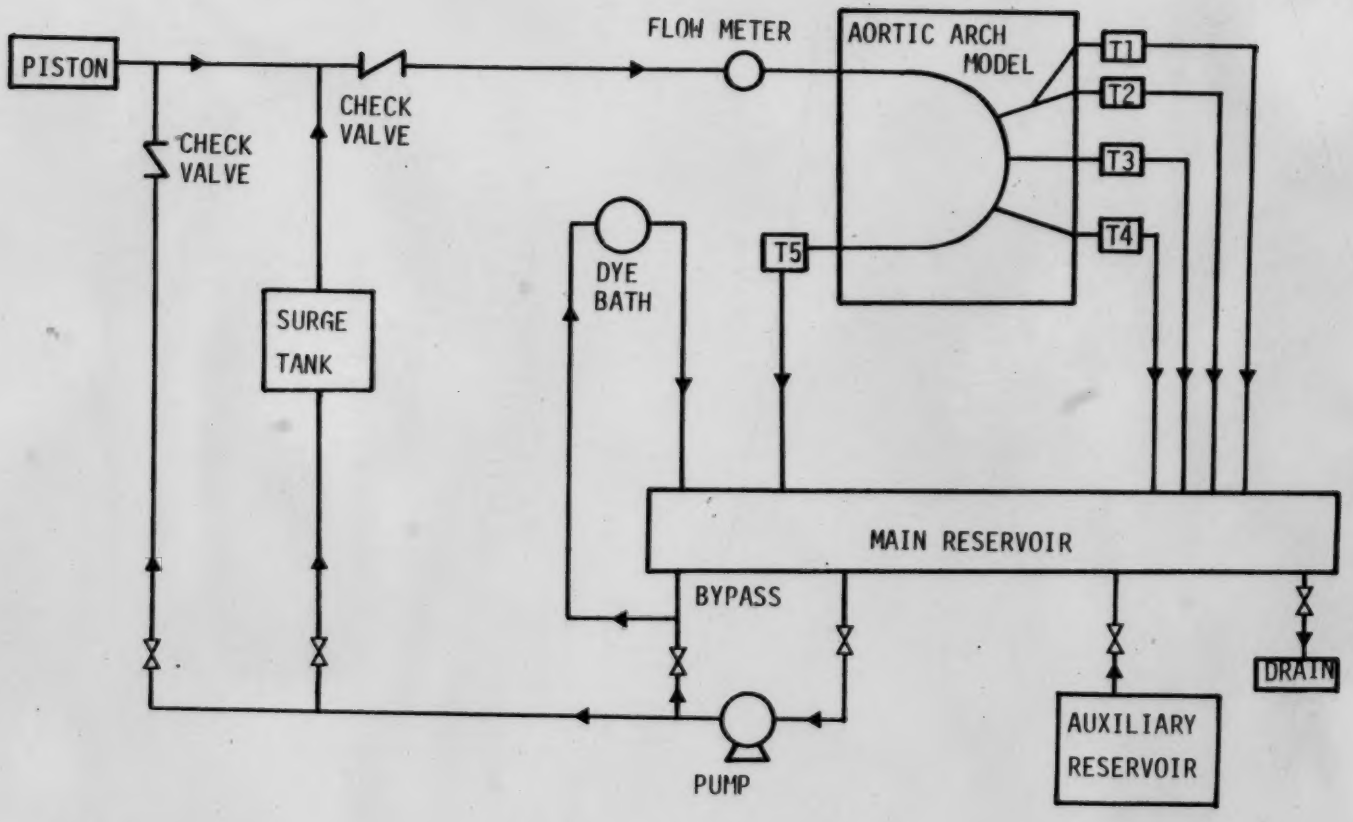

Figure 5.1. Flow Circuit

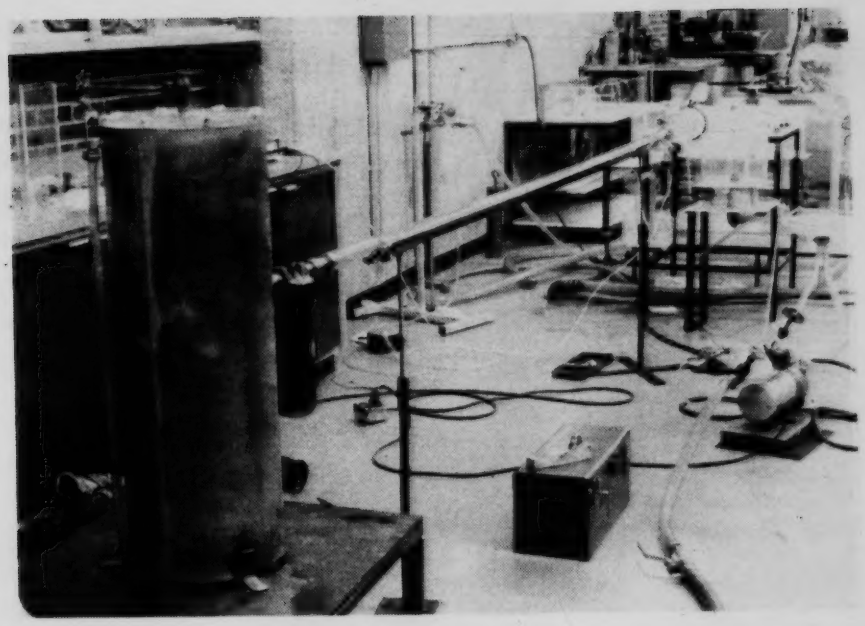

Figure 5.2 Experimental set-up

Figure 5.3 Model A

Figure 5.4 Fabrication of model A

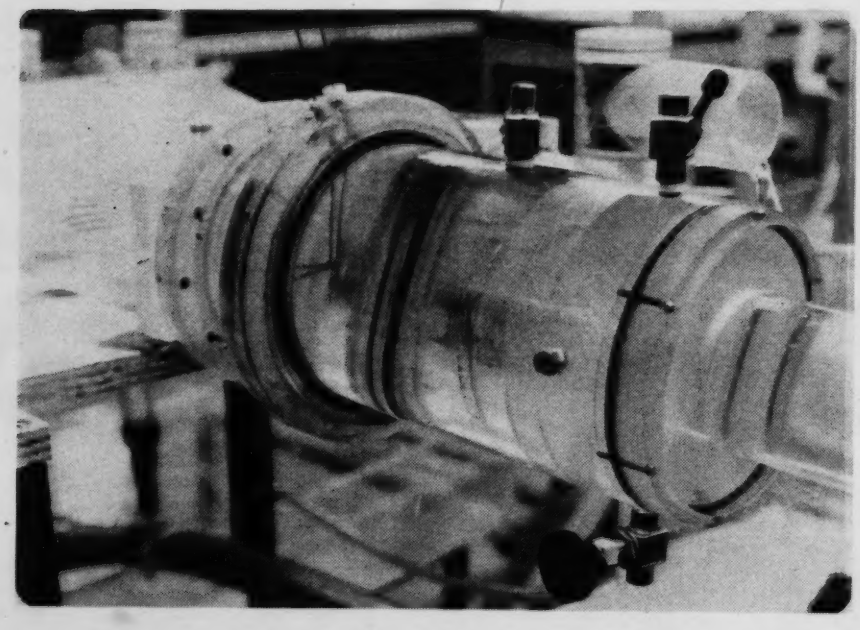

Figure 5.5 Model A inlet section

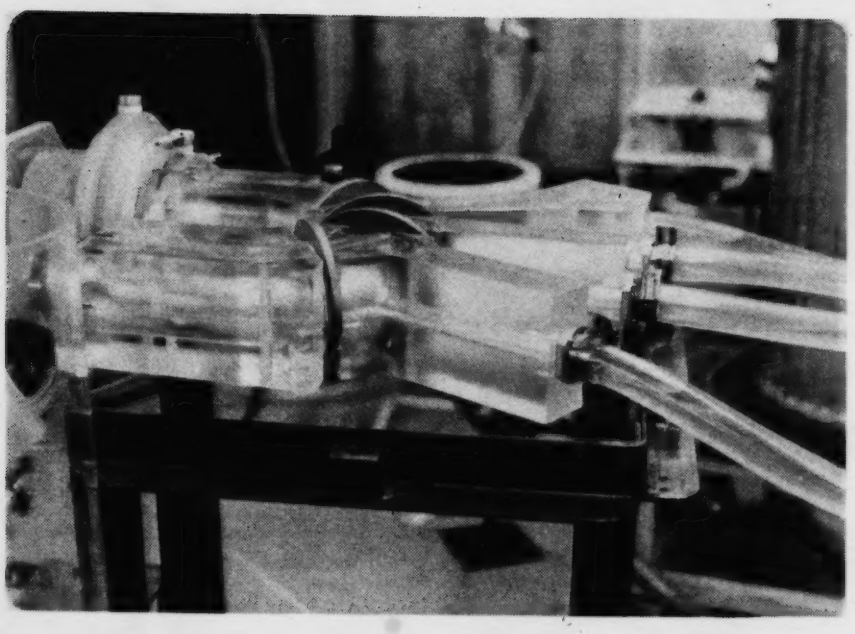

a.

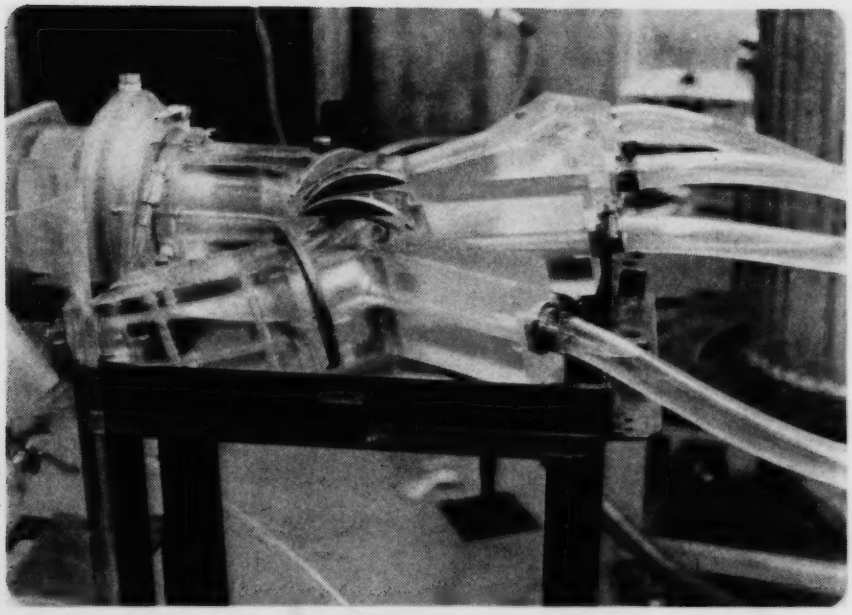

b.

Figure 5.6 Model B with and without twist

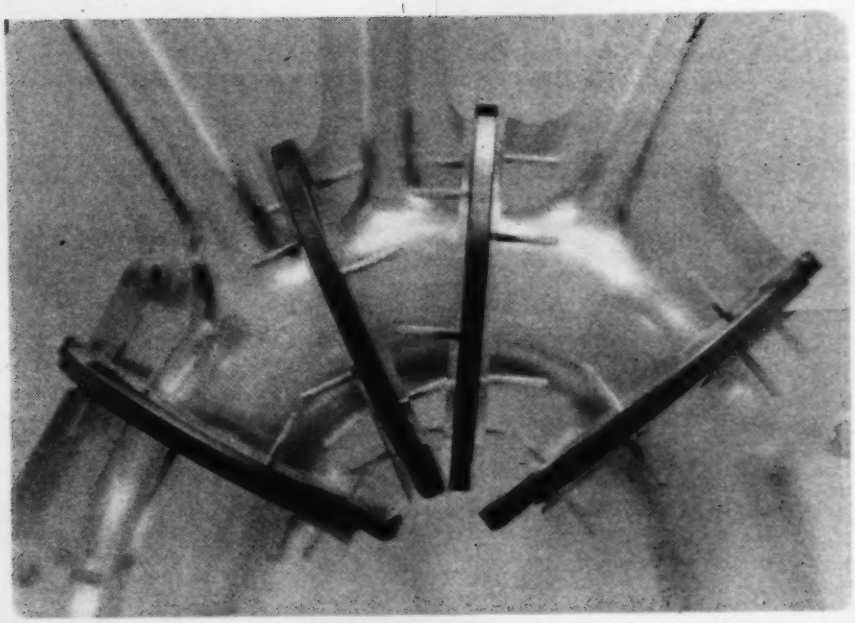

Figure 5.7 Model B rotatable sections

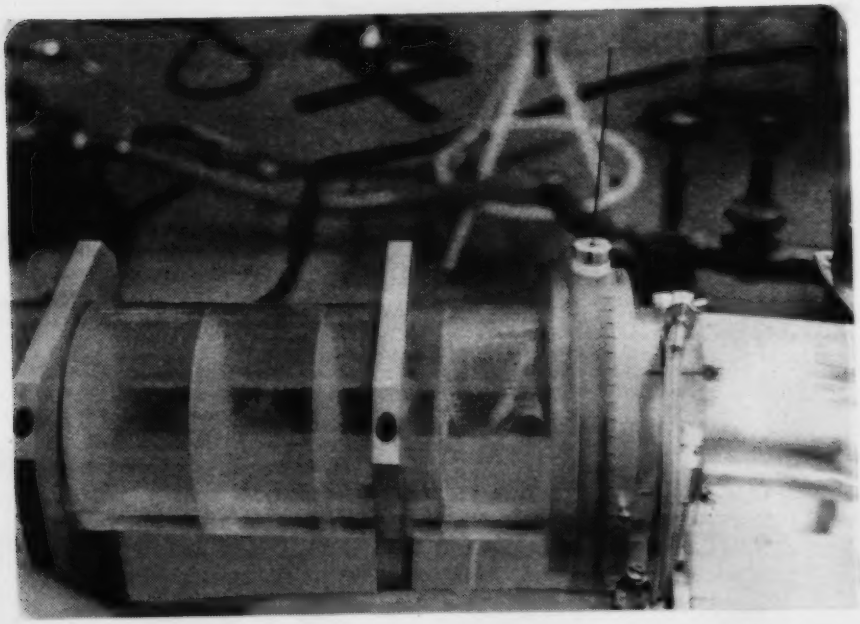

Figure 5.8 Model B inlet section

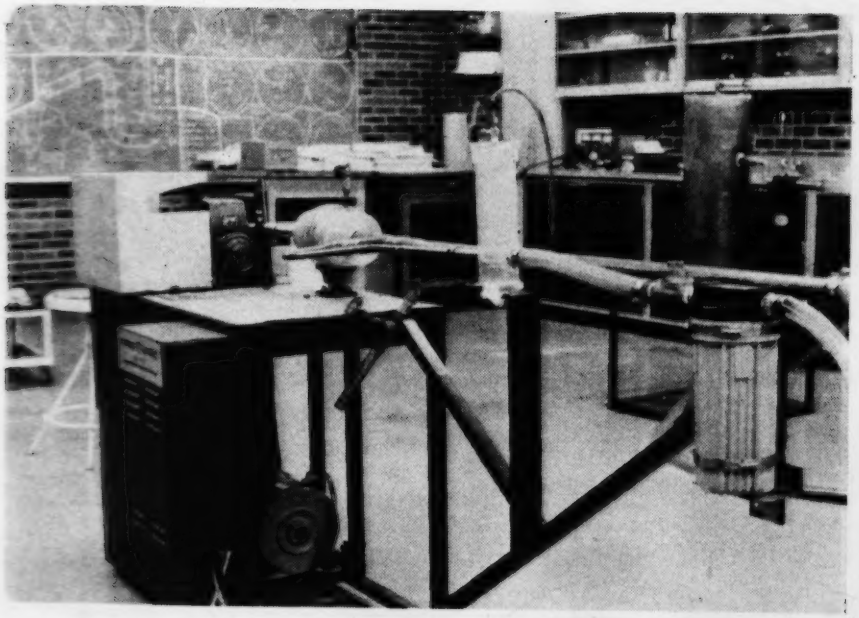

a.

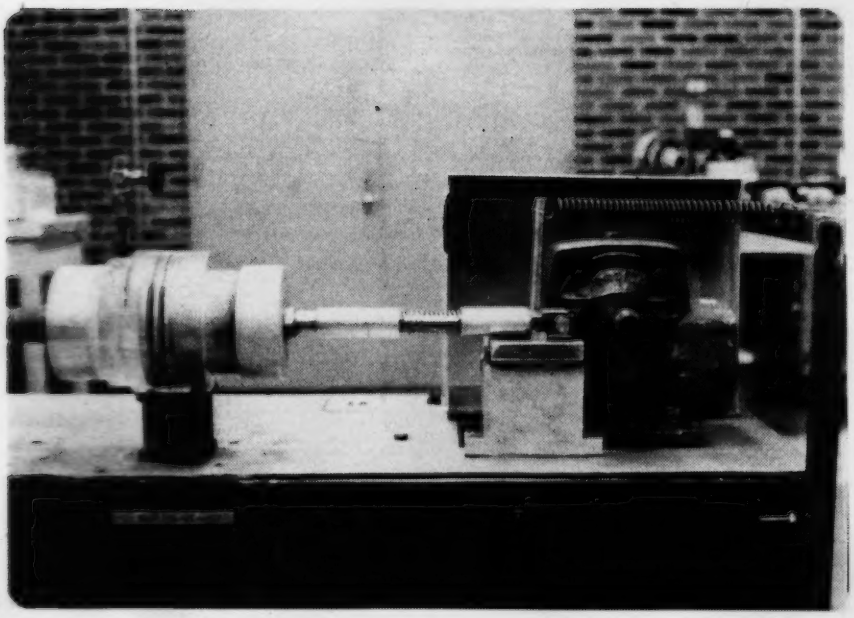

b.

Figure 5.9 Pulsation apparatus

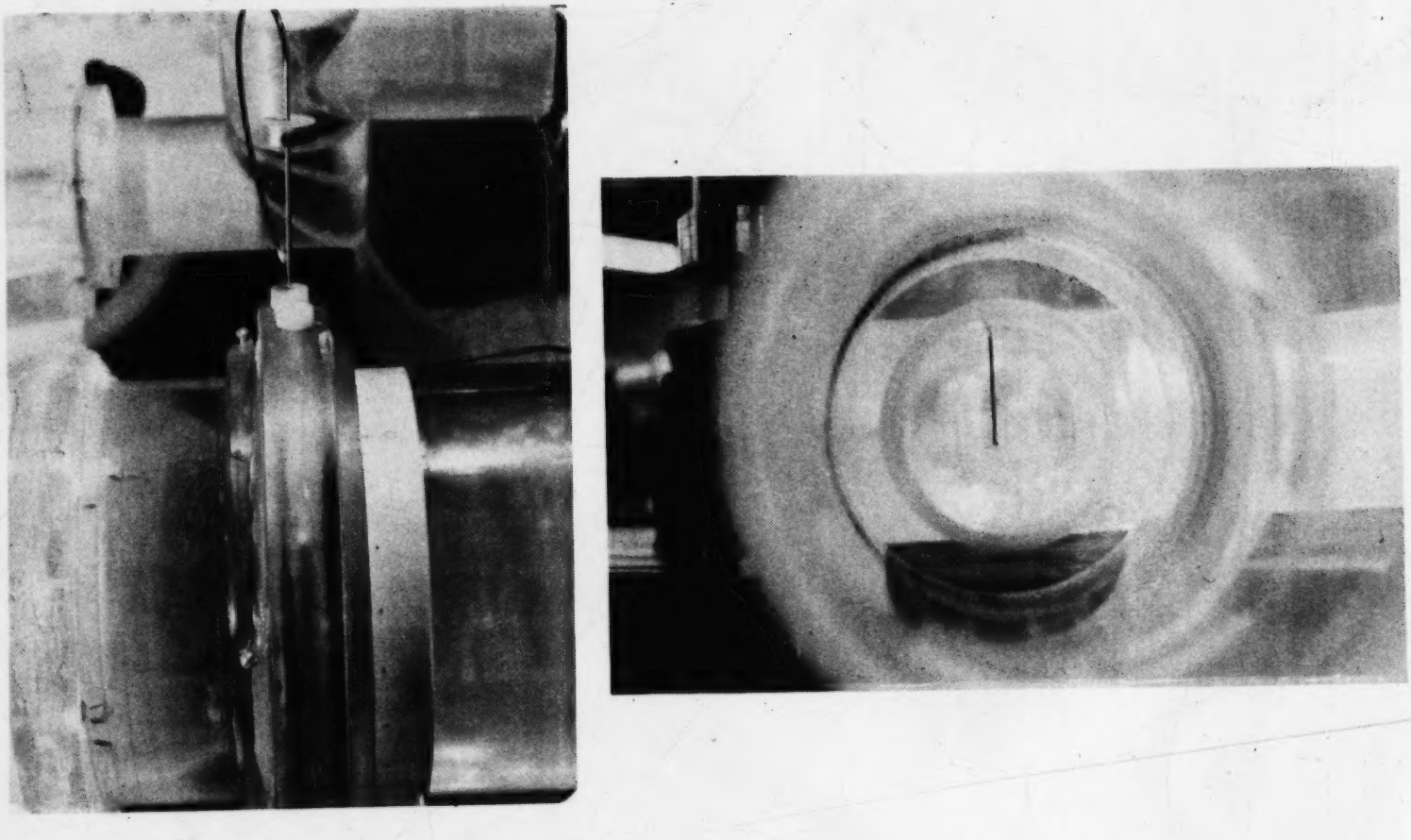

Figure 5.10 Dye pipe at inlet

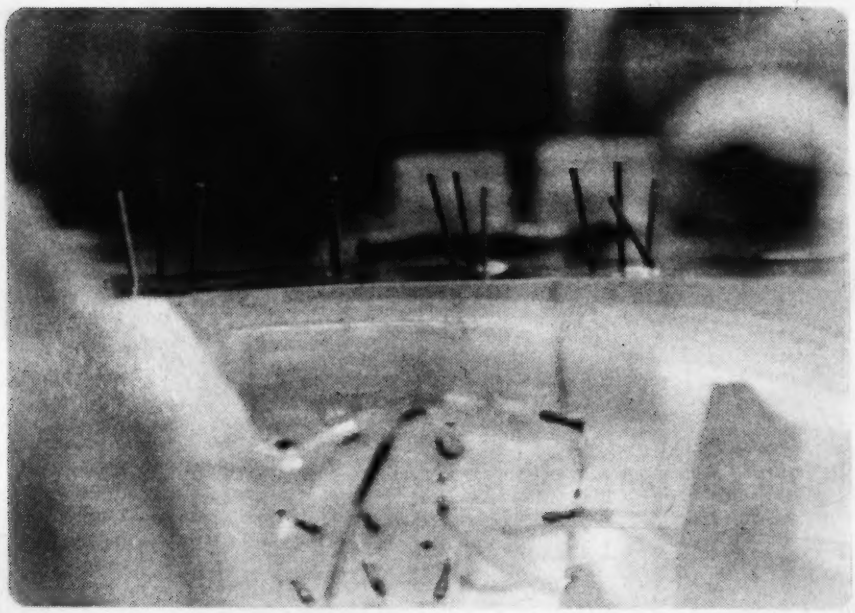

Figure 5.11 Peripheral dye pipes

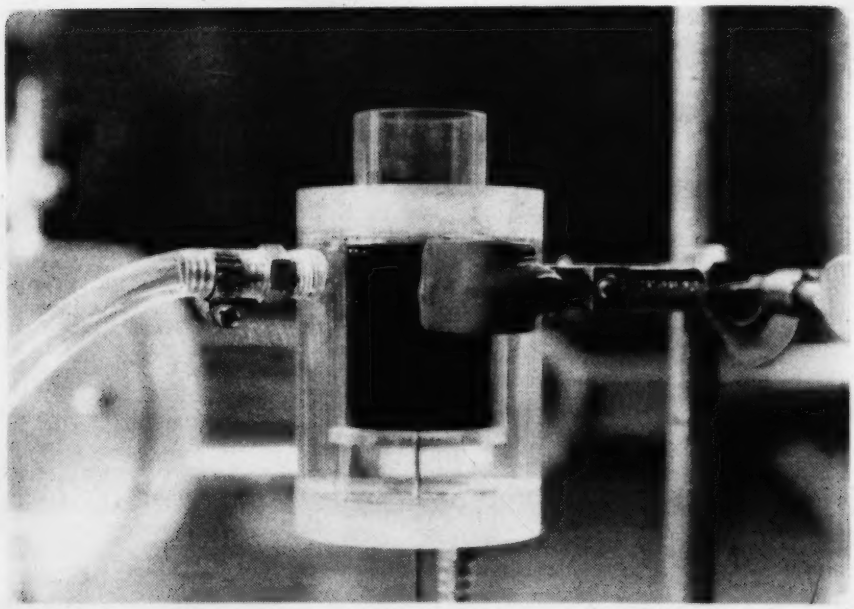

Figure 5.12 Dye reservoir bath

6. Shear Stresses in Derivative Branches

One of the important considerations in the study of blood flow involves the effects of wall shear stress. Several investigators have demonstrated some possible correlations between shear stresses and physiological phenomena such as hardening of the arteries (Fry,1968) and sites of incipient atheroma (Rodkiewicz,1975). However, there is no definitive proof of these relationships since the biochemistry of these problems is not yet completely understood.

Although shear stresses are not a major issue in this thesis, certain results have led to speculation about them which would require further substantiation. Therefore, part of the ensuing discussion attempts simply to provide leading questions for future research in this area.

6.1 Flow Partitioning

The flow distribution in each branch as a percentage of total flowrate is a strong function of Re as shown in Figure 6.1. This data was collected by choosing an orifice plate for each outlet which would produce the appropriate distribution at Re=1000 and then setting the flowrate to several Re values. These results concur with earlier data obtained in a single branch model (Rodkiewicz et al.,1976c) which demonstrated that the percent flowing through the branch decreases with increasing Re for steady or pulsatile flow.

In actual elastic arteries, the average differential partitioning of blood among organs is controlled by neural and hormonal stimulation hence the functional relationship is much more complex than in a rigid model. However, for a given physiological state, say at rest, the average resistance in each branch should remain more or less constant, with the instantaneous resistance primarily a function of flowrate, as in the plastic model. Consequently, if the flowrate in an actual arch were steady, the trend indicated in Figure 6.1 should apply.

Given the pulsatile flow nature, one can speculate that the same effect would occur based on the instantaneous Re. Hence at peak systole, a larger percentage of the total instantaneous flowrate would pass through the descending aorta (branch 5) than at other instants during systole. A schematic of this effect is shown in Figure 6.2.

Farthing and Peronneau (1979), having monitored the velocity profile in dogs' aortae, derived average flow versus time curves for each branch. By comparing flowrates in the branches at various instants, it was hoped that those results would concur with the above assumption. However, on closer inspection it would appear that their plots are faulty. The peak flows in a single upper branch exeeds the peak flow at the inlet and the sum of the net forward flows in the branches exceeds by far the net flow through the inlet.

Another study by Rodkiewicz et al.(1976a) considers the effect of the frequency parameter α on the flow distribution

with a constant net forward flow. Unfortunately there is a large data scatter and the results are not clear. Suffice it to say that these issues have not fully been clarified.

6.2 Factors Affecting Shear Stress

For steady flow in straight circular tubes, the wall shear stress τ_w, is proportional to the velocity gradient dv/dr. As the flowrate in a given tube increases, τ_w increases also.

Relating this to the aorta, as peak systole is approached, the instantaneous flowrate in all five branches is increasing as is the wall shear stress. However, since the percentage flowing through each upper branch is decreasing, the shear stress is increased less than if the percentage had remained fixed. Therefore the varying percentage distribution tends to damp the wall shear stresses in the upper branches and increase them in the descending aorta.

To get an idea of the relative magnitudes of the wall shear stresses in the various branches due to the net forward flow, consider the case of Poiseuille flow through a circular tube where:

$$v = \frac{2Q}{\pi R^2}\left[1 - \frac{r^2}{R^2}\right]$$

$$\therefore \tau_w \propto \frac{Q}{R^3} \qquad (6.1)$$

where r is the radial distance measured from the central axis and R is the tube radius. Table 6.1 shows the magnitude of the wall shear stresses due to net forward flow in the branches, estimated by the above equation and given as a percentage of the inlet wall shear stress.

Unfortunately, the effects of the instantaneous forward flow interact non-linearly with the pulsatile shear stresses. Given a certain sinusoidal forcing function $\frac{dp}{dt}$ exerted on the fluid in a circular pipe, the wall shear stress decreases as α increases (Fig.6.3). The relative magnitudes of the velocities at one point in the cycle for several α's are shown in Figure 6.4.

In section 4.8.2 it was shown that a value of α=19 is a representative value at the aortic arch inlet. However, since α is proportional to the pipe radius R, one can define a different alpha for each branch as:

$$\alpha_{branch} = \frac{R_{branch}}{R_{inlet}} \cdot \alpha_{inlet} \qquad (6.2)$$

The values corresponding to each branch are shown in Table 6.1. The lower values of α found in the upper branches would tend to raise the maximum wall shear stress due to fluctuations.

To summarize, the wall shear stress in the upper branches are somewhat damped by the change in flow distribution but it would appear that this effect is completely overwhelmed by two other effects: the smaller α in the

Table 6.1 Pulsatile Shear Stress

Branch	Mean Radius (mm)	$\frac{\tau_w \text{ (branch)}}{\tau_w \text{ (inlet)}}$	α
1A	6.1	1.48	8.0
1	3.7	2.40	4.8
2	3.8	3.89	5.0
3	3.8	3.89	5.0
4	4.5	1.34	5.9
5	11.7	1.48	15.3

branches tends to increase τ_w (compared to the arch), and the shear stresses due to the net forward flow are much higher in the smaller branches.

The above speculations are oversimplified having neglected wave reflections, secondary flows, elasticity and other factors, but the gross effects are probably a good assumption and could lead to a better understanding of the flow phenomena. The relative influences of these factors cannot be predicted and would require a further experimental research.

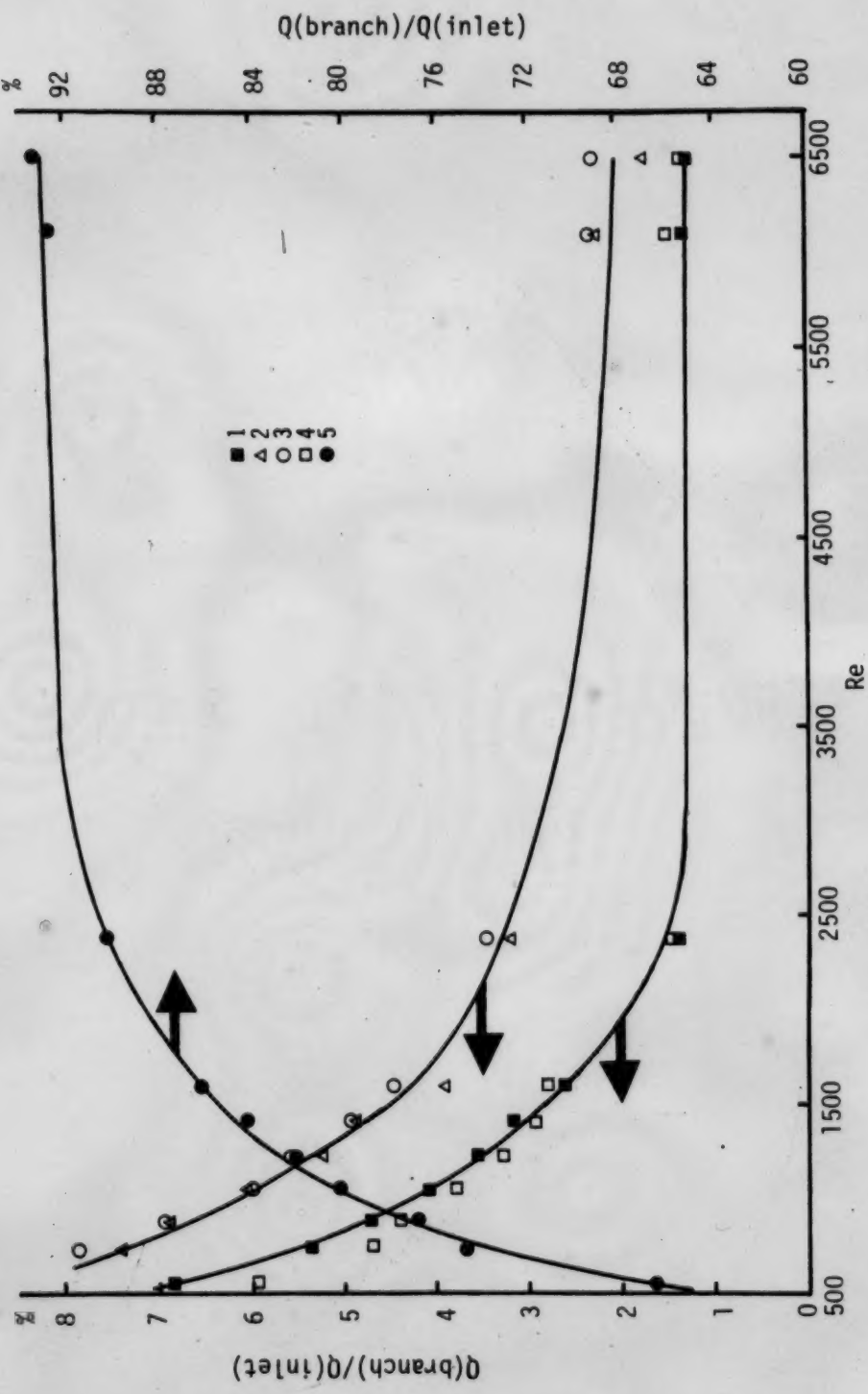

Figure 6.1. Flow Distribution Dependence on Reynolds Number

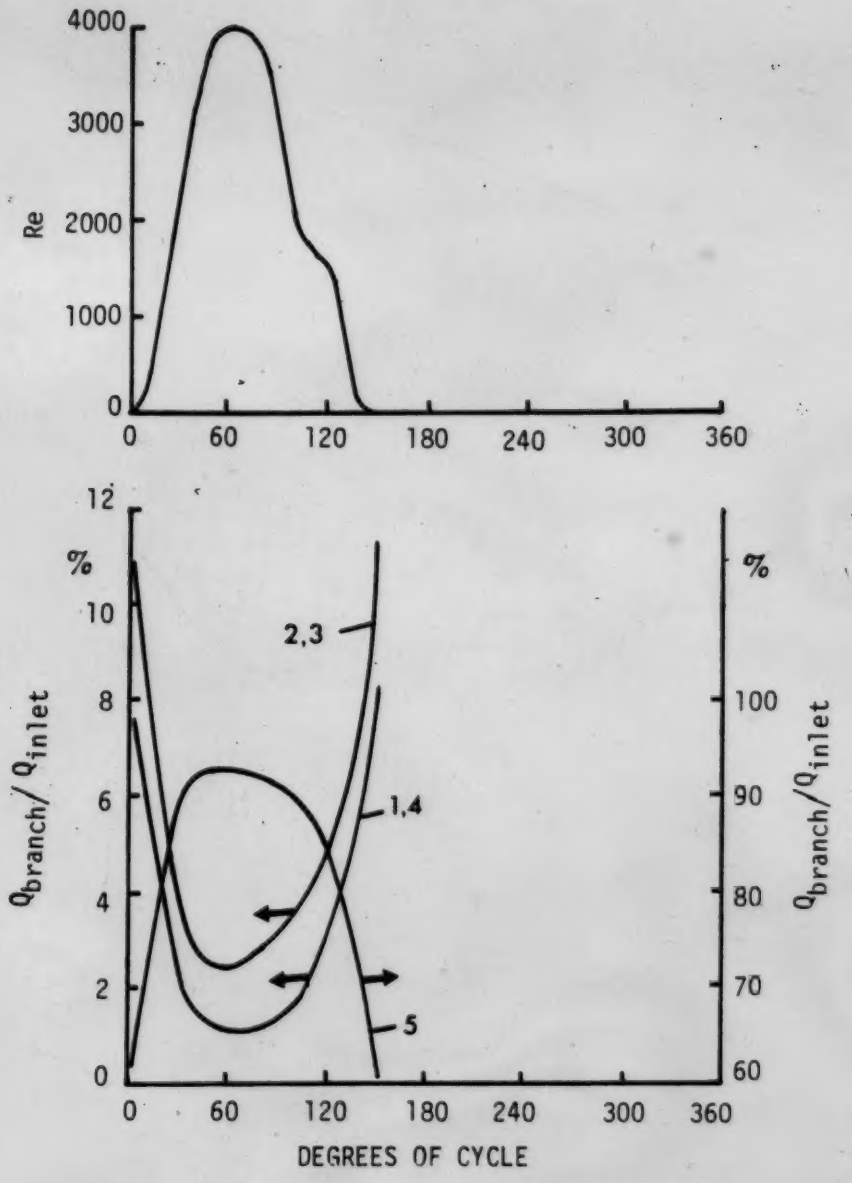

Figure 6.2 Variation in distribution during cycle

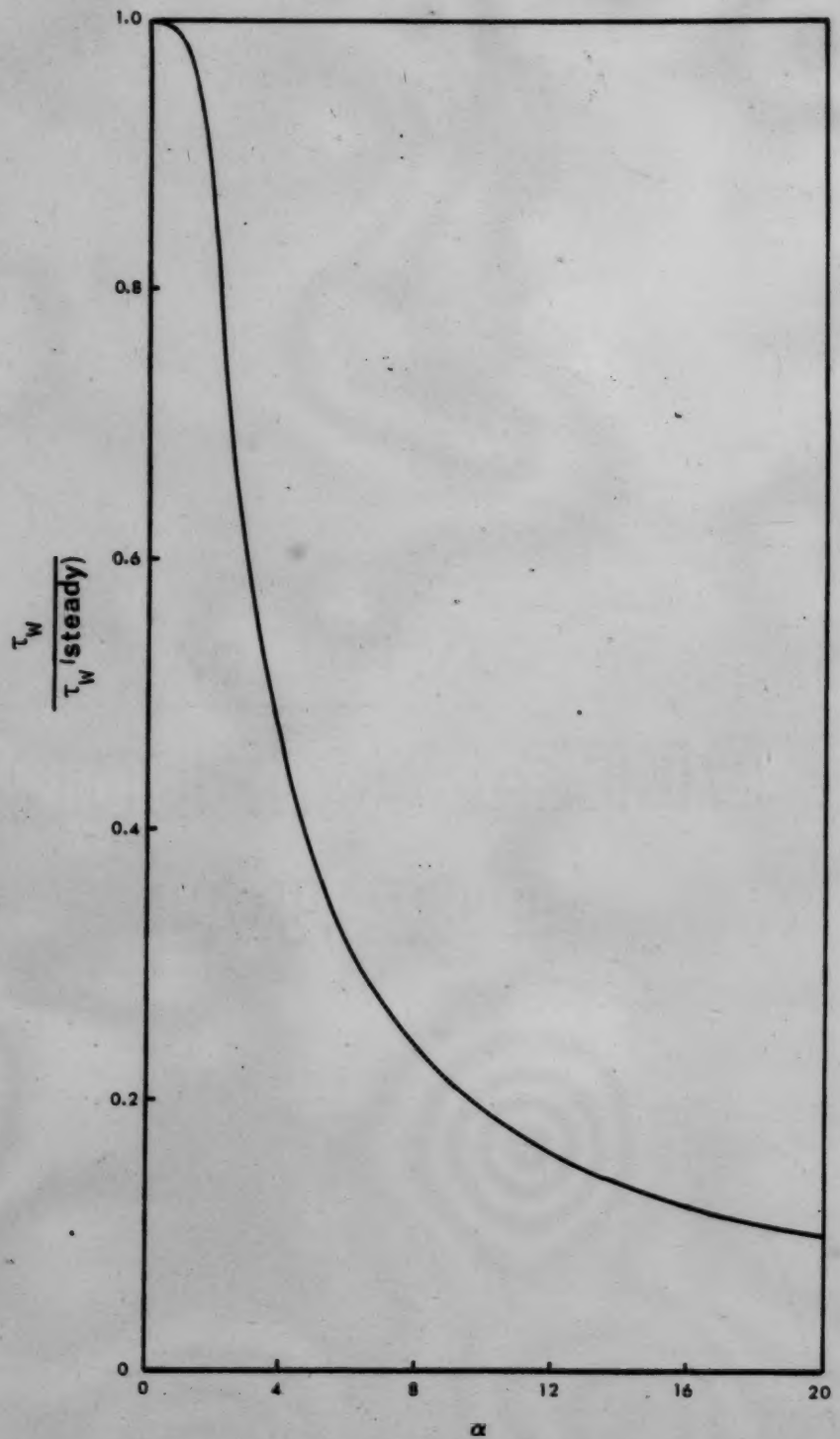

Figure 6.3 Effect of α on wall shear stress
(after Hildebrandt, 1981)

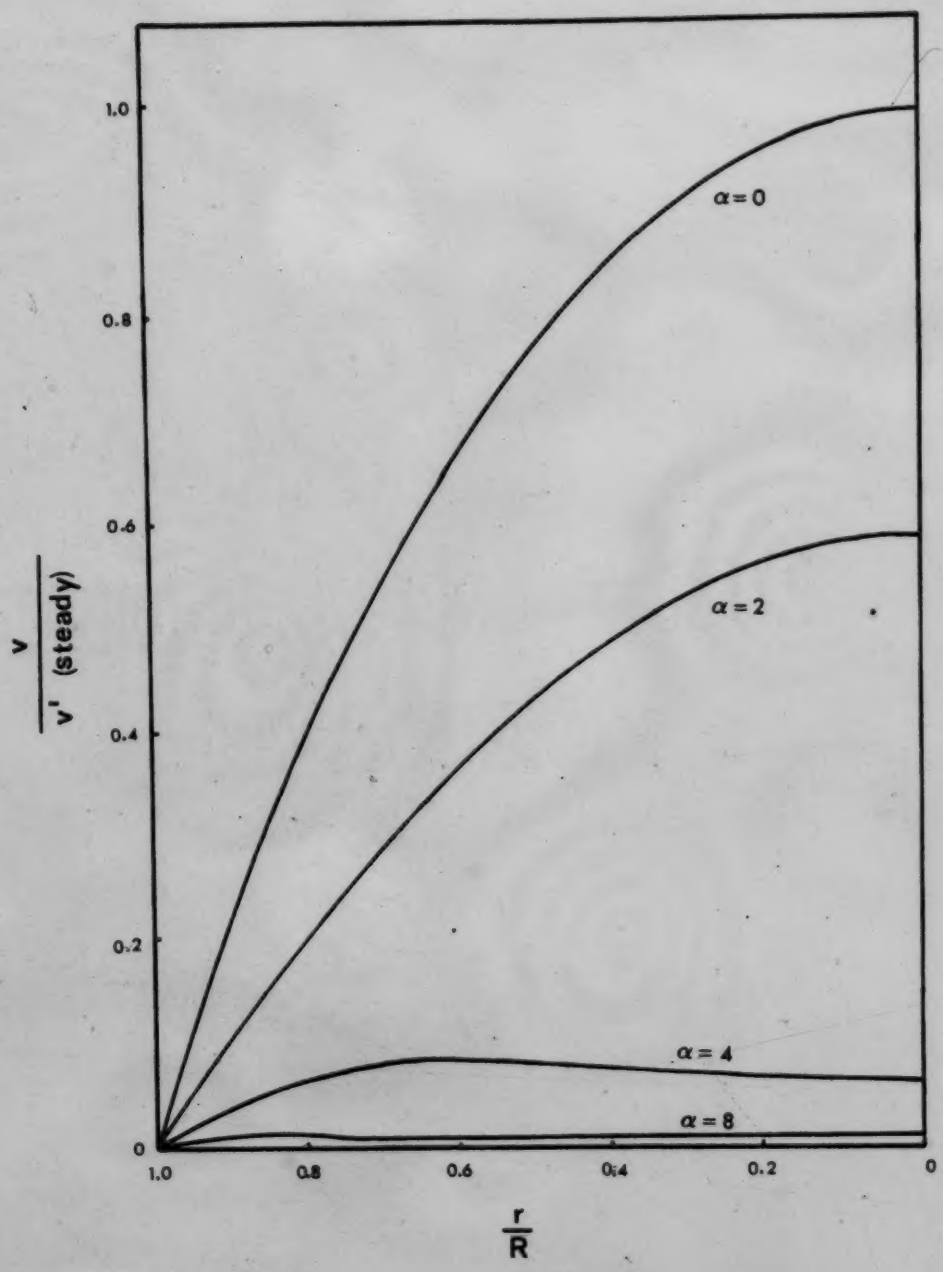

Figure 6.4 Effect of α on velocity profile(after Hildebrandt,1981)

7. Separation Zones

For the case of steady laminar flow, a separation zone can be considered as a region which cannot be reached by any streamline originating at the model inlet, unless flow instabilities are present. For pulsatile flow, this definition no longer rigorously applies due to the shifting of streamlines with time. However the basic concept that the separation zone constitutes a 'bubble' or captured vortex distinct from the main flow remains intact. Once the location of a suspected separation zone has been established, dye is injected directly into the area. Indication of reversed flow and persistance of dye presence in this region is accepted as further evidence of the existence of a separation region.

The existence and location of separation zones in the aortic arch and its derivative branches has long been a contested issue. As discussed earlier, present instrumentation cannot detect in vivo the localized flow reversals and vortices associated with separation zones. Also, since mathematical analyses are not refined enough to predict flow details at this level the only recourse lies in experimental models.

This report deals exclusively with two separation zones in the arch proper, although earlier studies have indicated the presence of zones in the major daughter branches as well. Figure 7.1 shows a dye stream in the main flow skirting a separation region in the brachiocephalic artery

on the proximal wall just distal to the entrance. The great majority of the tests were performed with steady flow since flow visualization with dye can be difficult under pulsatile conditions. Initial observations did not provide concrete evidence of reverse flow but were tantalizing nonetheless. In suspected separation locales, the flow would occasionally reverse only for an instant, leaving doubt whether the cause was some aberration rather than a feature of the flow. It was surmised, correctly, that Re=1000 was an approximate lower bound at which separation was initiated. As the Reynolds number was increased to 1400, the separation zones became more pronounced and regular. Raising the Re in the model to study separation can be justified on the basis that Re peaks near 5000 during pulsatile flow. Also the oscillations alter the mechanism behind separation such that flow reversal in these zones persists even throughout diastole (Re=0) so that the limiting value of Re at which separation occurs is primarily of academic interest.

7.1 Inner Wall Separation

The first separation zone occurs along the inner curve of the arch, near the plane of symmetry and approximately opposite the left carotid artery (Fig.7.2). The presence of this region is clearly indicated in Figures 7.3(a to f) by sequential photographs of flow reversal near the point of maximum curvature. The main flow proceeds from left to right

in the pictures and the dye is injected through wall tap number 37 (Appendix IV). The photographs are taken at 5 second intervals which, combined with the scale drawn on Figure 7.3a, indicates the slow progression of the reversed fluid. The velocity of the reversed flow is typically about 4% of the axial core velocity. This low velocity causes some dye to accumulate near the injection point and as the concentration increases the dye tends to diffuse slightly in every direction. This high concentration zone appears of the photographs as a small dark area around the injection point.

The dye stream in Figure 7.3 can be easily misinterpreted without the benefit of a side view. However, due to the constrained area at the inner curve of the model, the camera could not be adequately positioned for a feasible picture of the vertical plane. Therefore, a description and sketches are used to complement the photographs to provide a complete flow picture.

The apparent trajectory of the dye stream away from the inner wall is partly illusory. In effect, during the backflow period the dye is rising and following the arch wall quite closely. The thickness of the zone is actually about 3-4mm.

When the dye reaches the apex of the separation region most of it is entrained by the main flow and becomes entrapped in the inner wall vortices generated as a result of secondary flows (Section 8). Hence the forward flow depicted in Figure 7.3 takes place away from the wall.

Depending on which streamline the dye enters, some dye may follow the separation bubble to its point of reattachment.

Note that no recirculation is evident in the photographs. The dye is injected into the fluid layer nearest the wall which, when reaching the separation line, forms the interface between the main flow and the separation bubble. Due to minor instabilities in the flow, this layer continuously shifts slightly with the tendency to diffuse and mix the dye with the main flow. Injecting the dye with a higher momentum to reach the inner layers of the separation bubble is not practicable since the dye stream completely disrupts the flow in the area and observations become invalid.

It is very difficult to ascertain the location of the reattachment point since the clearance between the dye and the wall cannot be properly visualized. However the results of two other tests provide a good indication of the reattachment point location. Dye introduced at the next injection point downstream (tap #43) does not exhibit reversed flow so the separation does not extend that far. Dye injected upstream skirts the separation region and deflects back towards the inner wall about 0.5 centimeters past tap #37 (Fig.7.4). So, although the separation zone is not distinctly deleanated, an approximate range for this Re(1400) is from 1.5cm. upstream of the injection point to 0.5cm. downstream. In dimensionless coordinates this range extends from S/D=3.40 to 3.64 (Appendix IV). A schematic of the inner wall separation zone is given in Figure 7.5. The

widening of the zone as flow reversal progresses is probably accompanied by a thinning of the region although this could not be detected in the tests.

Normally, flow separation is caused by an adverse pressure gradient. If the low momentum fluid in the boundary layer encounters a pressure increase that it cannot overcome, it separates from the wall. The continuous convergence of the aortic arch would tend to suppress separation as a decreasing cross-sectional area causes the velocity to increase and the pressure to lower. The mechanism behind the flow separation at the inner wall is therefore not immediately evident. One hypothesis which conforms with earlier observations attributes the inner curve separation to the presence of branches. Rodkiewicz and Kalita (1978) showed that for a constant diameter curved tube with no branches and $400 \leq Re \leq 1800$, separation occurs only if the Reynolds number is large enough and the radius of curvature small enough. They also considered curved tubes with a side branch for both the cases of constant diameter and convergence of the main branch. In both cases separation on the inner curve was observed but it was not indicated at what Reynolds number. They state however that, as expected, convergence decreases the size of the separation region and prevents its appearance for small Re. Scarton et al.(1976) also tested a model geometrically similar to the arch but without side branches. He did not find any separation on the inner wall for the full physiological range of Reynolds number up to

Re=5700. Rodkiewicz(1975) also found a separation along the inner wall of an open channel model of the arch under pulsatile conditions. It was suggested by other researchers that the results were not definitive due to the difference of secondary flows between a channel and a closed tube.

The results of the present experiment in conjunction with the earlier works provides substantial evidence that the inner wall separation is caused by the existence of the large branches originating at the top of the arch. The separation is not due to the curvature of the arch alone nor to the influence of secondary flows, and the convergence of the aorta is obviously not enough to prevent it.

The presence of the branches increases the effective area of the arch thus increasing the pressure and giving rise to an adverse pressure gradient sufficiently large to cause separation of the slow moving fluid on the inner wall. The average velocity near the inner curve is lower than that on the side walls due to the influx of low momentum fluid by the secondary flow vortices. This explains why the side wall fluid does not separate.

7.2 Separation on the Outer Wall

The second separation zone occurs on the outer curve upstream of the first branch (Fig.7.2). This separation region is also initiated at a Reynolds number of about 1000. Its existence was suspected and searched for as a result of

earlier work by Rodkiewicz(1975) which demonstrated that this was also a site for atherogenesis, albeit a minor one. This separation region was also evident in the open channel flow model of the arch.

Figures 7.6a,b show a side view of the backflow indicated by dye alternatively injected through taps #1 and #3. Since the taps lie on the plane of symmetry of the model, the flow should divide evenly as in Figure 7.6a. However, small flow inconsistencies sometimes forced the dye to follow either the upper or lower vortex (Fig.7.7)

There is some speculation that this area is in fact not a separation zone but simply the site of a complex backflow pattern. The arguments in favor of a separation zone are that no external streamline was found to enter the region; the location corresponds to the separation found in the open channel model; there is no other plausible reason for backflow to occur in his area. The reasons for doubting separation are that no vortices are evident in the region (other than the large secondary flow vortices); the dye does not reattach but is swept away (perhaps due to the fact that it is in the outer streamline); there is no obvious mechanism to induce separation at this location. With the data available it is not possible to gain further insight into this phenomenon pending further investigations.

7.3 Separation in Periodic Flow

The observations made for the steady flow case do not explicitly confirm the existence of the separation zones under pulsatile conditions. Preliminary pulsatile tests were performed with a minor backflow period as in the physiological situation. The flow near the walls tends to reverse more easily than the core flow under pulsatile conditions since the momentum in the boundary layer is lower. This effect is shown in Figure 7.8. So although backflow was still present in the previously defined separation regions, it also occurred at almost every other wall tap examined. To compensate for this, the input waveform was somewhat modified so that the average flowrate remained positive throughout the cycle. The amplitude varied from a minimum of Re=50 to a maximum of Re=4000. The flow in the separation areas was then compared to that at several other wall positions.

Due to the many components in the flow circuit, it was deemed wise to monitor the pulsations to ensure that the proper waveform existed at the model inlet. The output from the Annubar flowmeter recorded on an oscilloscope is presented in Figures 7.9a,b. The first picture indicates the fundamental sinusoidal input from the cam using a low-pass filter. The second figure represents the actual unfiltered waveform. The origin of the high frequency noise is not known but it is not equal to the blade passing frequency of the pump. Two plausible explanations are the noise from the Annubar due to the pulsatile input or wave reflections from

the model which is just downstream from the flowmeter.

It was found that the flow everywhere in the arch except in the separation regions either continued forward or virtually stopped as the inlet flow reached a minimum. In the separation zones the converse occurred. As the inlet flow attained its maximum the flow reversal at the wall became almost non-existent and as the flowrate decreased the fluid in the separation zone surged upstream forming a large backflow area. This effect was also observed in the open channel model by Rodkiewicz(1975). One possible explanation of this phenomenon is the variation in flow distribution with Re (Section 6.1). As the inlet Re is decreasing, a larger percentage of the flow is diverted through the branches thus effectively lowering the pressure in the arch in that region and causing the low momentum fluid at the inner wall to surge backwards.

The effect of these cyclic variations is that the blood exerts a fluctuating stress on the arch walls, particularly in the separation zones. The elastic walls deform accordingly but eventually may lose their resiliency due to the large alternating shear stresses. This phenomenon may contribute to the development of arteriosclerosis and subsequent atherogenesis as the wall metabolism is disturbed and fatty lesions begin to develop.

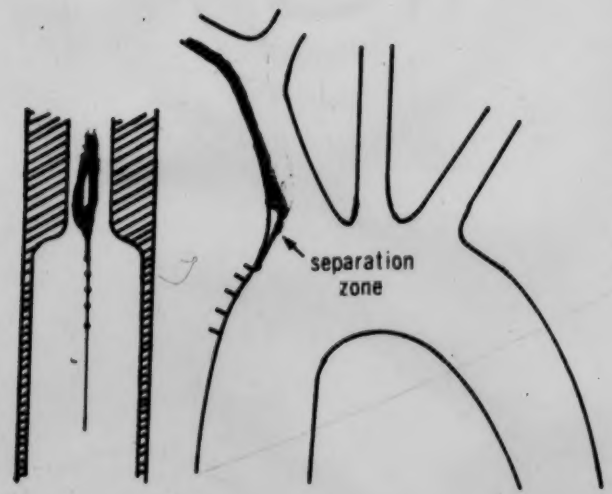

Figure 7.1 Separation in the brachiocephalic artery

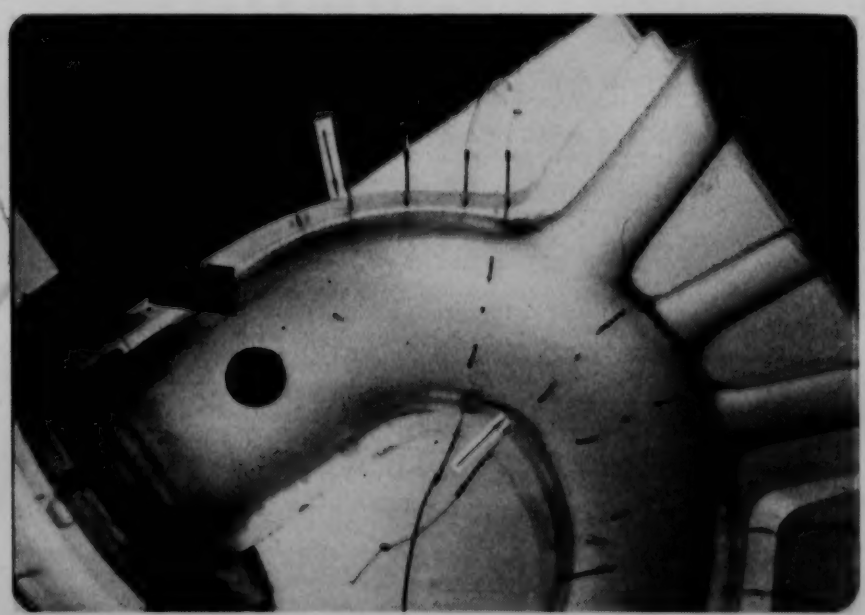

Figure 7.2 Location of arch separation zones

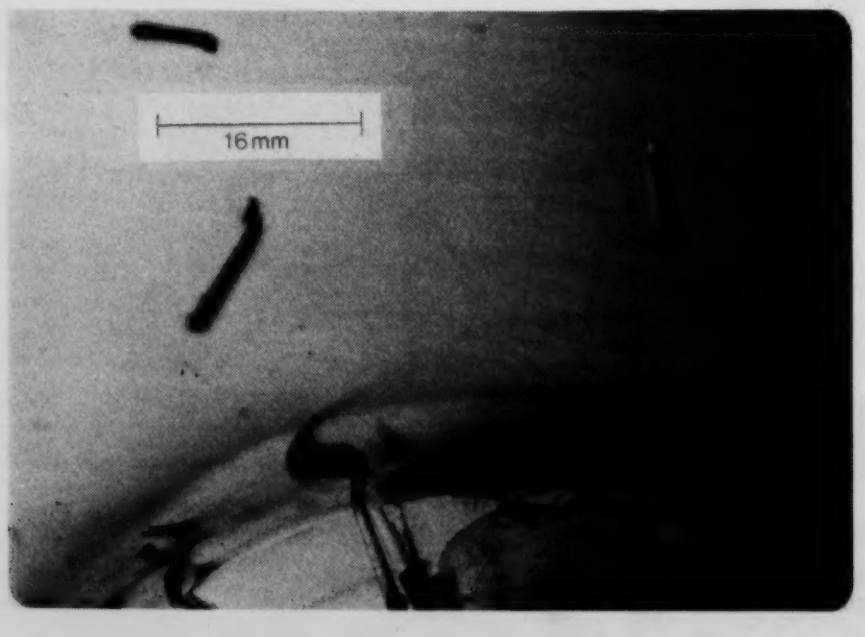

a.

b.

Figure 7.3 Progression of inner wall backflow

c.

d.

Figure 7.3 (continued)

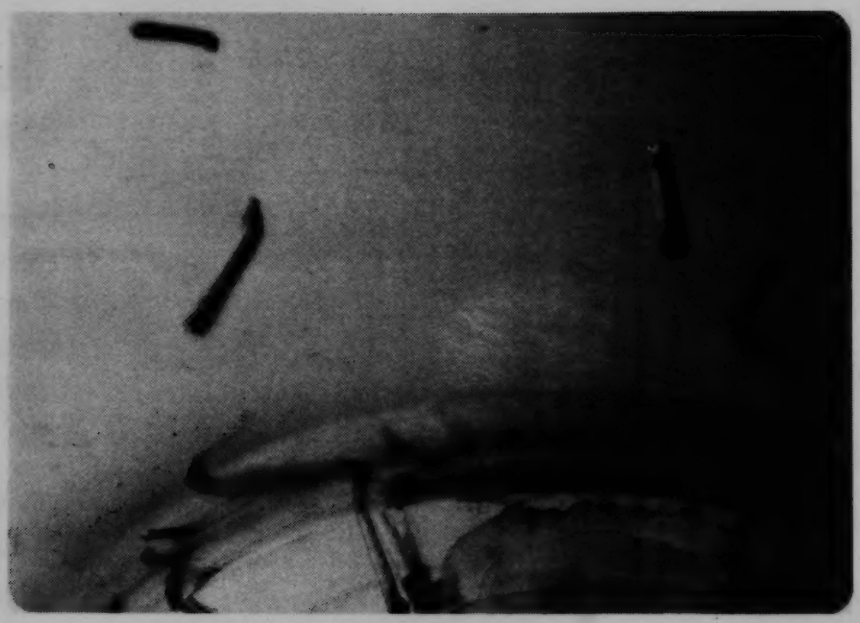

e.

f.

Figure 7.3 (continued)

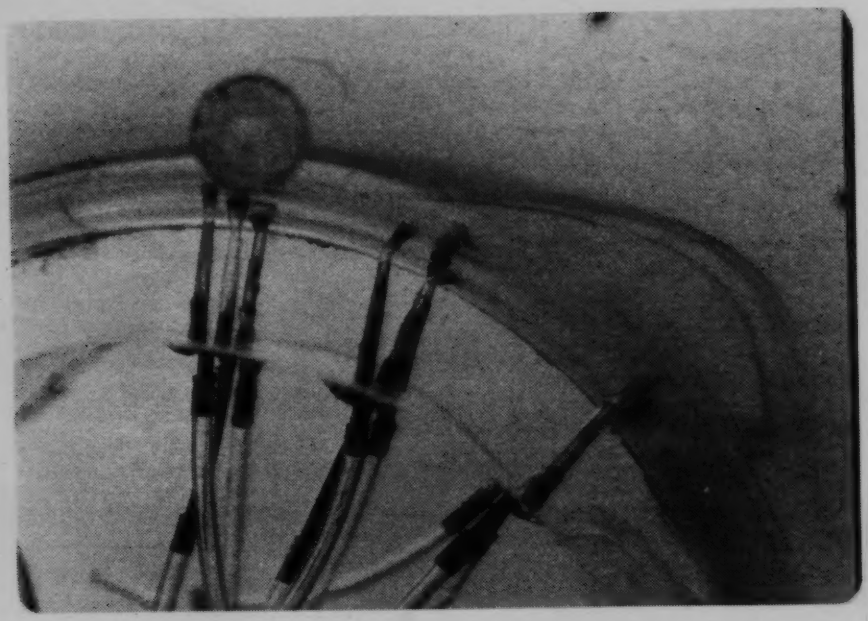

a.

b.

Figure 7.4 Main flow bypassing inner wall separation

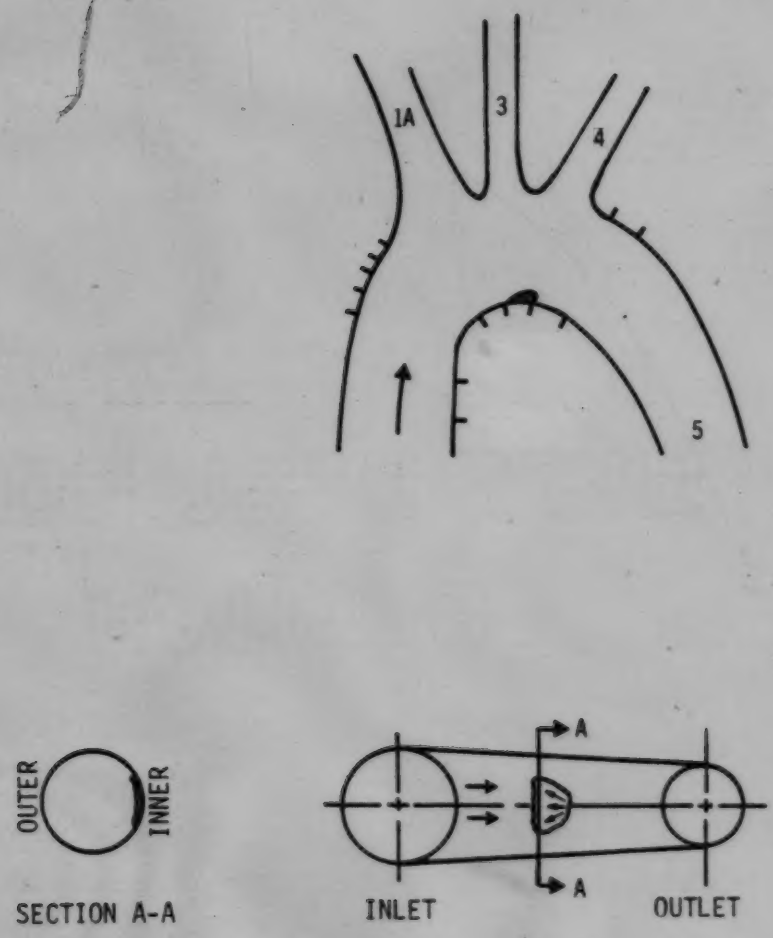

Figure 7.5 Three views of inner wall separation

a.

b.

Figure 7.6 Backflow along outer wall

a.

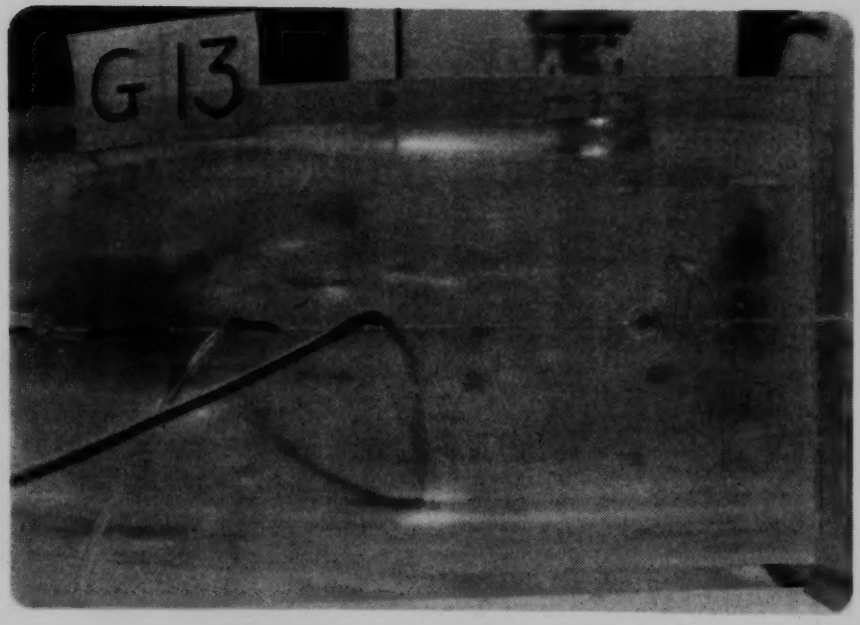

b.

Figure 7.7 Upper and lower vortices

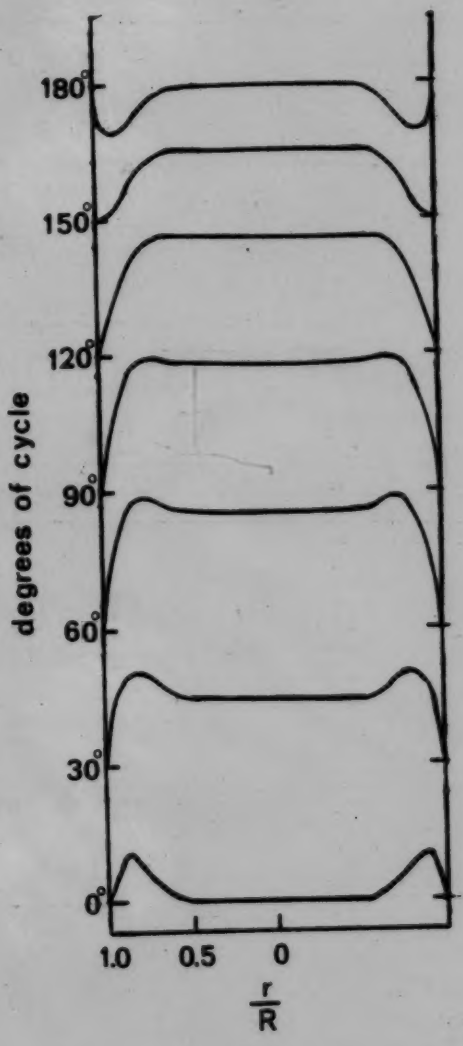

Figure 7.8 Velocity profiles at several times(after McDonald,1974)

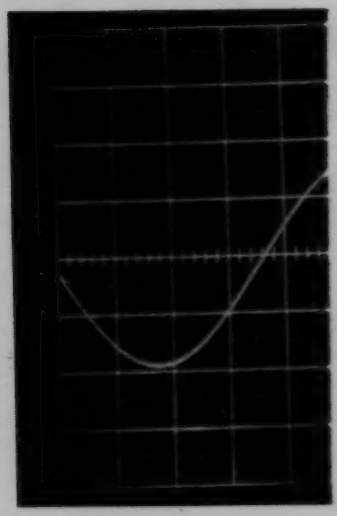

Figure 7.9a Filter

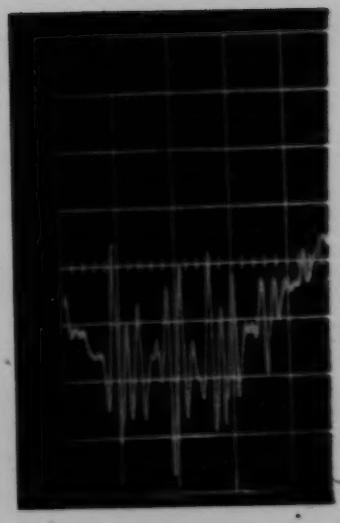

Figure 7.9b Actual filter

8. Flow Patterns

The flow characteristics of the aortic arch include some well-studied patterns such as the large scale vortices associated with secondary flows and several finer points which even detailed observations yield grudgingly. Most of the testing was performed under steady flow conditions but the effects of pulsations were considered when possible.

The flow patterns are examined from two points of view. The approximate paths of the fluid particles from the inlet are determined and then more detailed aspects of the flow are studied by injecting dye through the wall taps. The major characteristics of the flow are the potential core, the boundary layer vortices and the branch flows.

Since the branches affect the flow a great deal, a mapping of the source of the fluid destined to pass through an upper branch is useful in determining their effect on the main arch flow. A record of the positions of the inlet dye pipe corresponding to a branch streamline produced the mapping shown in Figure 8.1. The three areas labelled 1A, 3 and 4 represent the fluid which flows respectively through each of the three upper branches. The flows through the right subclavian and right carotid are conveniently lumped into one region (ie.1A, brachiocephalic artery) for two reasons. The dye has often become quite diffuse once it has attained the bifurcation in the brachiocephalic artery, particularly if it is in the boundary layer making it difficult to ascertain its ultimate destination. Also, the bifurcation

occurs quite far from the arch where the actual artery has already twisted quite a bit (Fig.4.1), hence the geometric similarity of the model is poor in this location. Knowledge of the destination of various inlet streamlines could also prove useful for injecting substances into the aorta to enter a particular branch. Branch flow is shown in Figure 8.2.

Although the boundaries between the regions are distinct in Figure 8.1, this is not representative of the experimental results. When the dye is injected in the interior of any of the regions the results are consistent. However, dye injected near the boundaries of these areas often fluctuates between the two adjacent branches and occasionally three. In theory, the distinction should be clear and the boundaries separating the areas would correspond to stagnation lines between the branches (Fig.8.3). However minor fluctuations in the flow cause these limiting streamlines to vacillate. A quick check on the data is performed by noting that the branch area in Figure 8.1 represents about 22% of the total area which corresponds to the distribution set for the branches.

As predicted, the boundary layer has not completely developed by the outlet of the model and therefore a core of fluid remains inviscid during its passage through the arch (Fig.8.4). The slowing of the fluid in the boundary layer is accompanied by a velocity component inward towards the axis and under this influence the core fluid accelerates. By

injecting two dye streams side by side, it is seen that in this potential flow region the velocity is lower the farther one gets from the center of curvature although no quantitative data was collected in this respect. The potential core region shrinks as the boundary layer thickens and occupies about 20% of the outlet area compared to 100% at the inlet.

The area in Figure 8.1 labelled 'core' represents the fluid which remains in the potential core during its passage through the arch. Note that the whole area is potential at the inlet and that a much larger area than that marked 'core' remains inviscid for at least part of its course.

The remaining unlabelled region in the figure represents the fluid which becomes part of the boundary layer or becomes part of a secondary flow vortex. The large gap between area 1A and the outer wall indicates the amount of fluid which is displaced peripherally towards the inner wall before the first branch is reached since none of this fluid enters the brachiocephalic artery.

As the boundary layer begins to grow and the fluid passes into the bend, the centrifugal force is higher on the faster core flow which is forced outwards. Consequently the outer boundary layer thins as fluid is forced peripherally to the inner wall. This effect is clearly shown in Figure 8.5 by dye injected into the boundary layer. Figure 8.6 shows streamlines which remain in the potential core for part of their trajectory and are then entrained by the secondary flow vortices. When observing along the arch

centerline facing downstream the upper vortex rotates clockwise and the lower vortex counter-clockwise. This behaviour is similar to fully developed flow through a curved tube except that the vortices do not return to the outer wall along the centerline. Rather they cannot penetrate the relatively high momentum potential core fluid so they remain as two trapped vortices along the inner wall (Fig.8.7).

The fluid which begins along the inner wall remains along the inner wall as the boundary layer thickens and when it is joined at the inner curve by the secondary flow from the outer wall, most of it becomes entrained in the trapped inner wall vortices. It is quite easy to visualize the outer wall vortices but when the inner wall vortices first form they are quite small scale and difficult to observe. Initial observations in this area appeared only as lateral fluctuations in the dye stream, whether viewed from above or from the side, which was originally attributed to irregularities in the inlet flow. However, lateral fluctuations which appear in both the horizontal and vertical planes can be caused either by fluctuations in an oblique plane or by a small scale vortex.

A mirror was mounted to attempt to photograph both views at the instant and resolve the issue. The results of this method were inconclusive. A second dye pipe at the inlet was used to inject another dye stream very close to the first one. These streams remained parallel for a certain distance and then began twisting around each other

indicating the presence of an inner wall vortex (Fig.8.8). The appearance of these vortices first occurs approximately opposite to the left carotid artery which is about the location of the inner wall separation zone. The inner wall vortices continue to grow as they proceed downstream and fill about half of the tube at the outlet.

The branches have some direct effect on the potential core by causing a more pronounced outwards displacement than that which would occur in the absence of branches. This in turn increases the magnitude of the outer wall vortices to replace the outward moving inner wall fluid.

Some observations were made under pulsatile flow conditions although the dye diffuses more easily. The vortices remain intact throughout a period of oscillation but the pitch lengthens and shortens accordingly, much as a coil spring would. Unfortunately, it is not possible to determine from the observations how the strength of the vortices is affected by the frequency or amplitude of the oscillations.

The outer wall vortices downstream from the branches are less pronounced than those upstream of the branches. There are two effects which contribute to this. The arch is starting to come out of its curve after the last branch and as the radius of curvature increases, the centrifugal effects lessen. The boundary layer is also quite thin on the outer wall having started over after the left subclavian stagnation zone. This means that the high momentum fluid is already near the outer wall and a significant secondary flow

is only induced once the boundary layer becomes thick enough.

Summarizing, the inner wall flow consists of a thick boundary layer and trapped inner wall vortices which begin near the location of maximum curvature. An inner wall separation zone is also located opposite the upper branches. The inner wall is therefore subjected to a relatively low shear stress and also to localized opposing stresses at the separation line. The inner wall is a prime candidate for atherogenesis, which can be attributed to depositions enhanced by the slow moving blood flow as well as wall damage incurred by separation zone stresses. Conversely, the outer wall upstream of the first branch is also subject to atherogenesis but there the flow is characterized by a local flow reversal and a thinner boundary layer hence a higher shear stress.

Two hypotheses could explain the above observations. Atherogenesis could be attributed either to shear streses that are too high (Fry,1968) or too low (Caro et al, 1971) as suggested by Scarton et al (1976). These conditions could be aggravated by the presence of flow reversal which could hamper the walls' defences. The second hypothesis assumes that atherogenesis sites coincide with the flow reversal regions and do not depend directly on the main flow shear stresses. This hypothesis is partly substantiated by the coincidence of atherogenesis sites and separation zones in the branches demonstrated by Rodkiewicz(1975).

There was no evidence of turbulence at any time, either for steady or pulsatile conditions. The transition Reynolds number in a curved pipe is normally higher than in a straight pipe, in the order of Re=5000 to 10,000. This depends a great deal on the curvature ratio of the tube. Nerem et al(1972) performing in vivo studies on dogs, made a rough estimate of the critical Reynolds number as a function of the frequency parameter α by inducing higher frequency pulsations with drugs. They found that $Re=150\alpha$ in the ascending aorta and $Re=250\alpha$ in the descending aorta. The value for the ascending aorta was measured very close to the aortic valve where disturbances from the heart may still be present. In the arch itself, which is the main area of concern in this study, $Re=200\alpha$ can be used as a reasonable estimate. For $\alpha=20$, the critical Reynolds number is in the order of 4000, so although no disturbances were observed in this test, the fluid may have been on the verge of transition during the pulsatile tests.

There is another important consideration in the study of flow patterns in the aortic arch. In certain circumstances when the carotid arteries become almost completely occluded and neither cleaning nor medications can clear the lesions and restore the flow, a bypass may be installed to circumvent the blockage. The bypass, normally a segment of vein, is usually attached to the aorta at a convenient nearby location. Often the bypass itself becomes occluded, sometimes with dire consequences. This could be caused by

the biochemical state of the individual's blood system. From the fluid dynamicists point of view however, there could conceivably be some advantages in selecting an optimum size, location and angle at which to install the bypass. The size of the vein used (if available) would preferably be sufficient to supply an adequate amount of blood to the deficient branch. The angle of attachment between the bypass and the aorta can affect the flow patterns and induce unwanted separation zones as shown by Rodkiewicz'(1973) studies of bifurcations. Optimizing the location of a bypass could also favourably affect the percentage of blood flowing through it as well as minimize flow disturbances.

As an initial guess, it was thought that locations of maximum pressure in the arch would be conducive to smoother flow into a bypass. Attempts to monitor the pressure differences between various wall points in the same plane resulted in the discovery that the differences were too small to measure with the equipment available. The taps were then bled in turn and the outflow collected over a long period of time to determine the maximum pressure locations. The differences in hydrostatic pressure from one point to another were compensated for by adjusting the heights of the bleed tube outlets. Although there were differences in volume collected after long time periods, it turns out that the differences were not significant and smaller than the errors induced by the experimental method. This test was therefore inconclusive.

To test the effectiveness of bypasses of various sizes and at various locations, a research program is presently underway to occlude some branches in the model and install bypasses. The study of flow patterns in and around the bypasses should indicate whether these parameters critically affect their function.

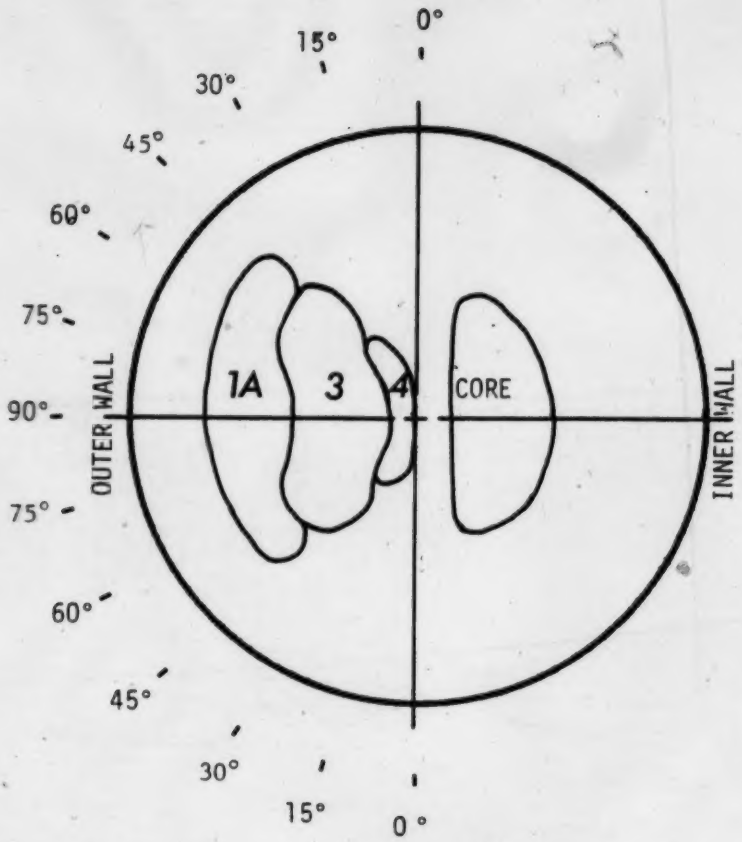

Figure 8.1 Destination of inlet flow

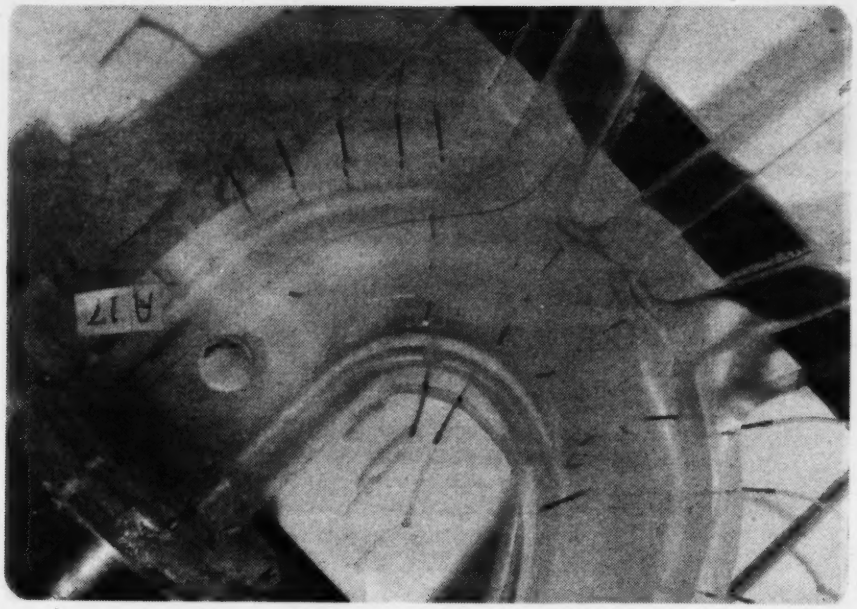

a.

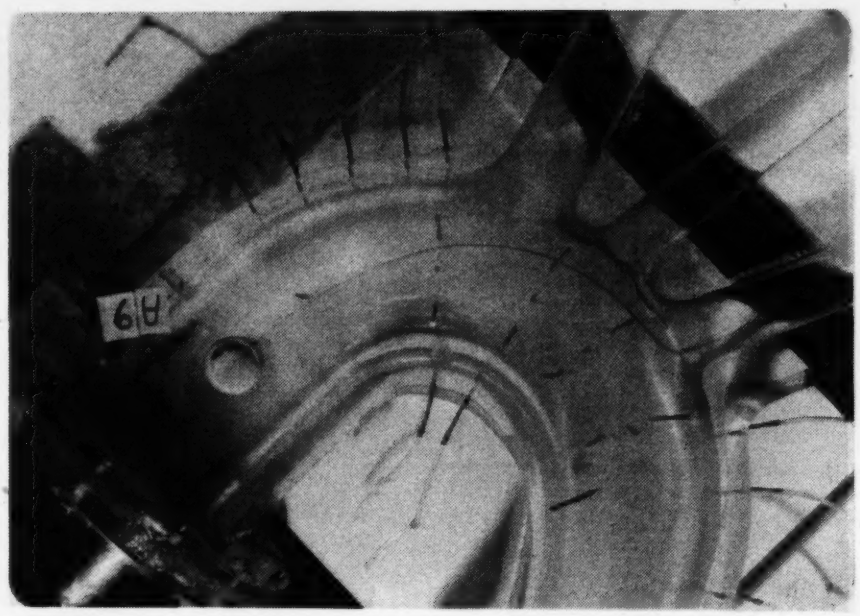

b.

Figure 8.2 Flow into the branches

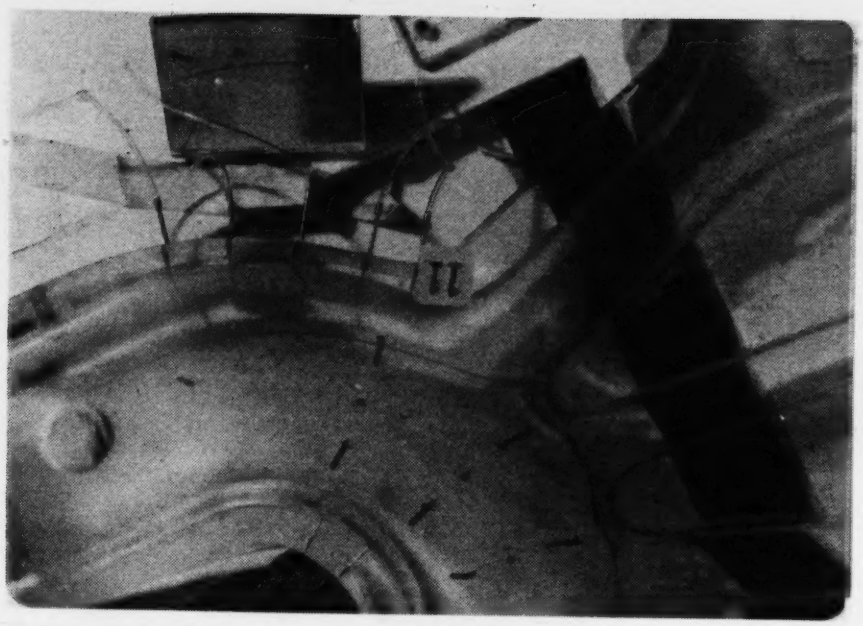

a.

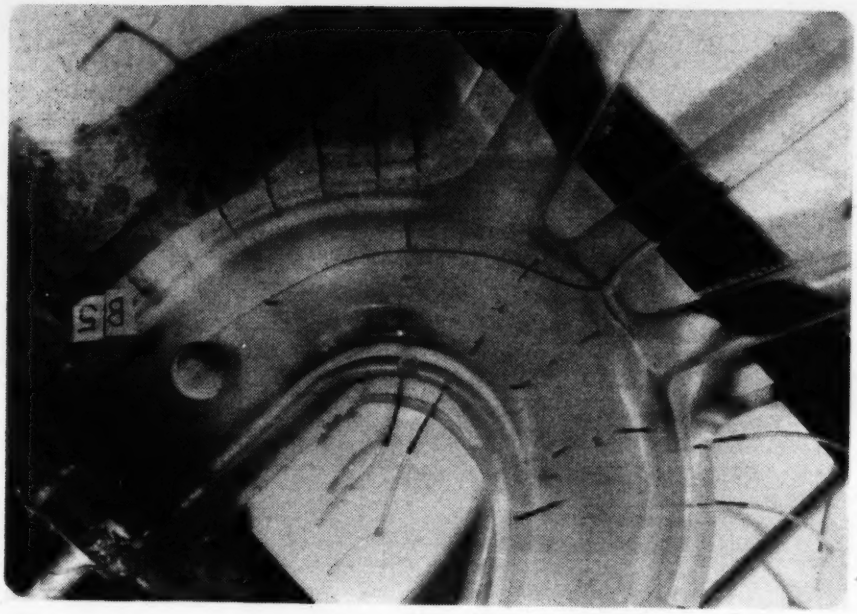

b.

Figure 8.3 Stagnation zones at branch inlets

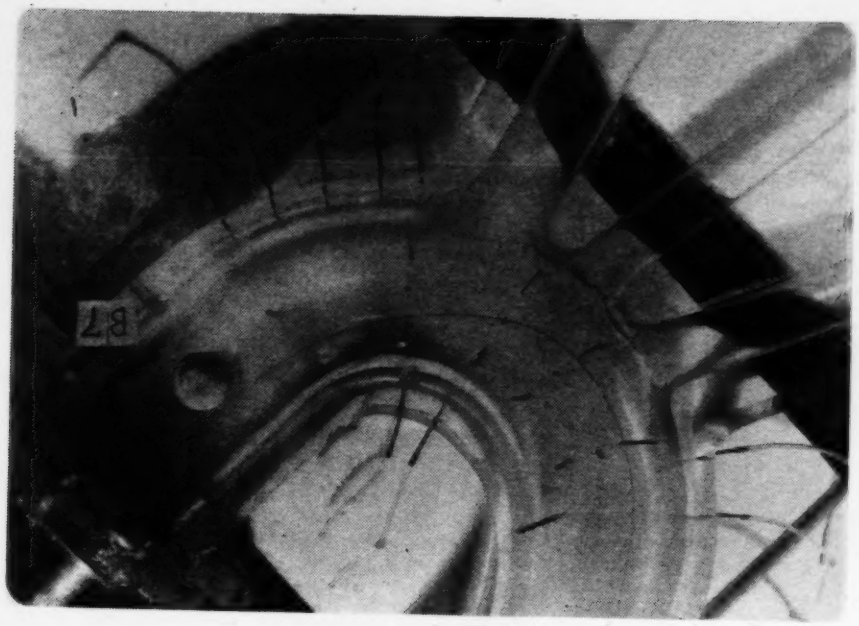

a.

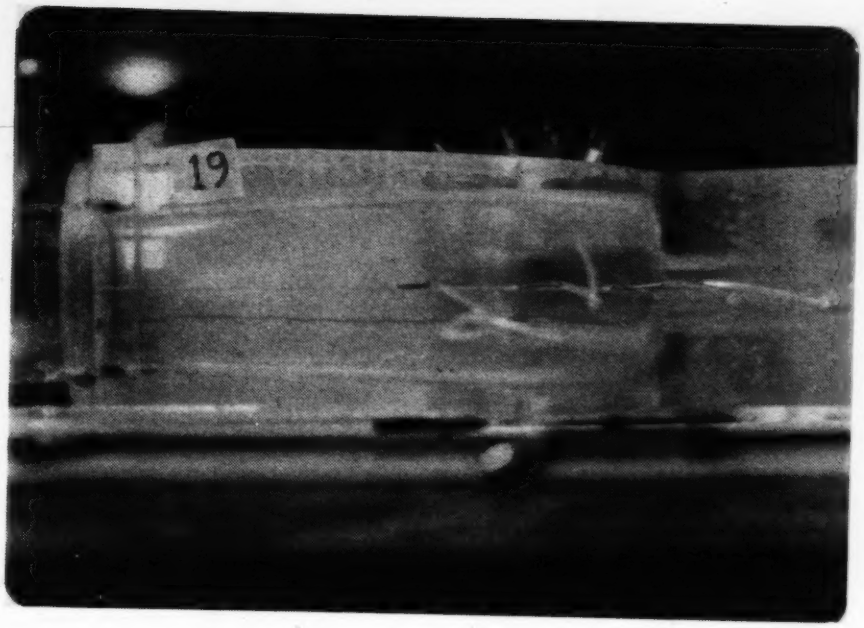

b.

Figure 8.4 Streamline in potential core

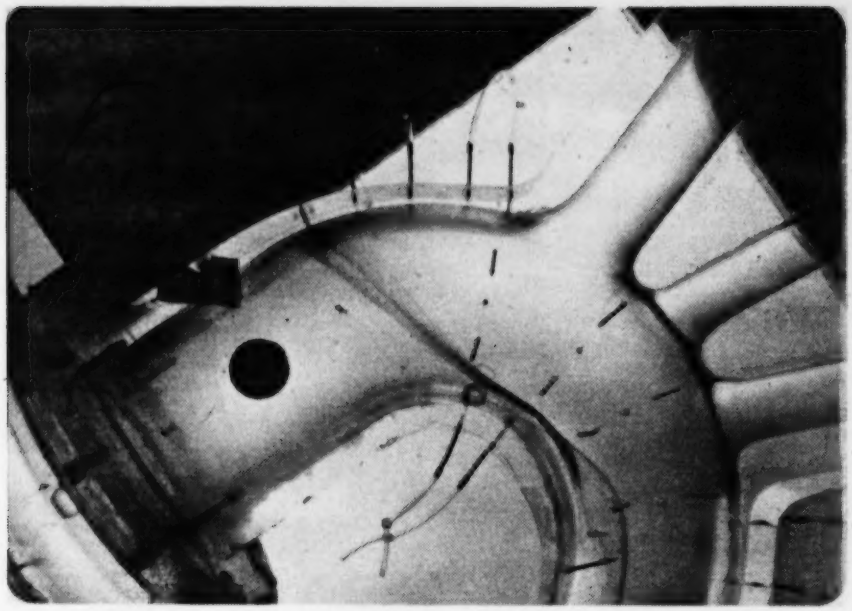

a.

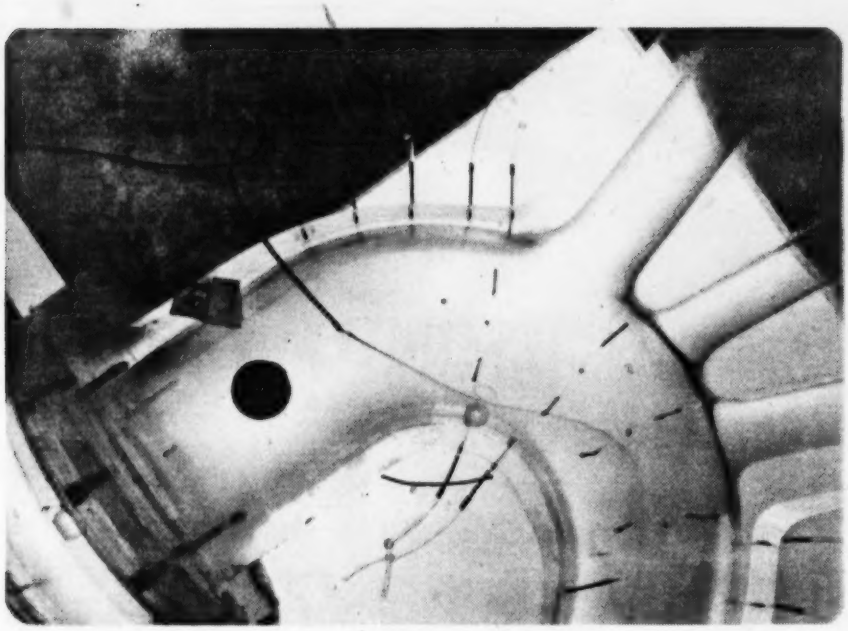

b.

Figure 8.5 Dye injected into secondary flow vortex

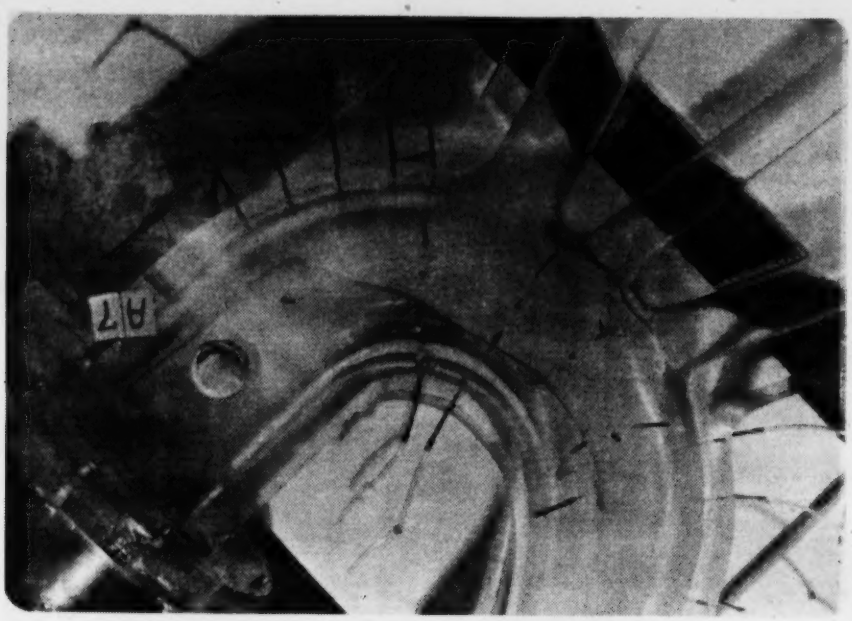

a.

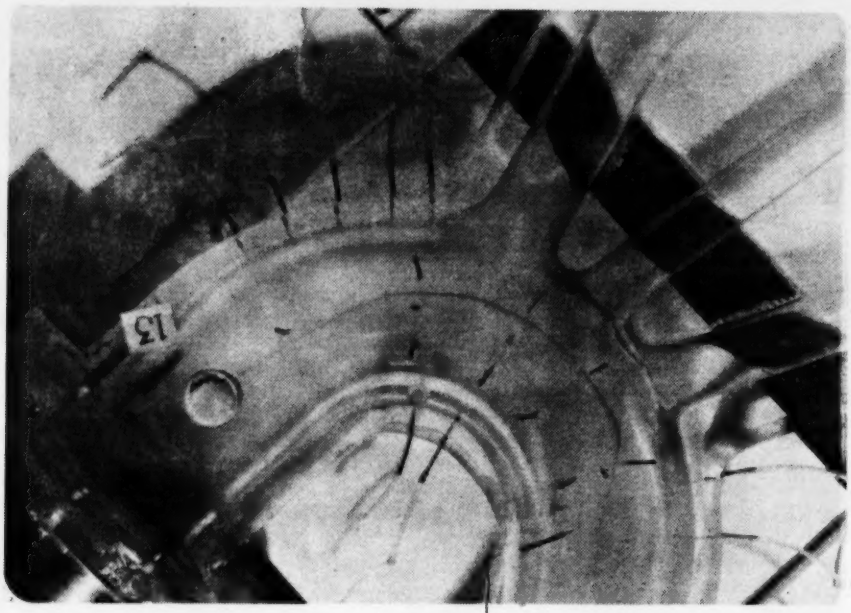

b.

Figure 8.6 Core streamline entering vortex

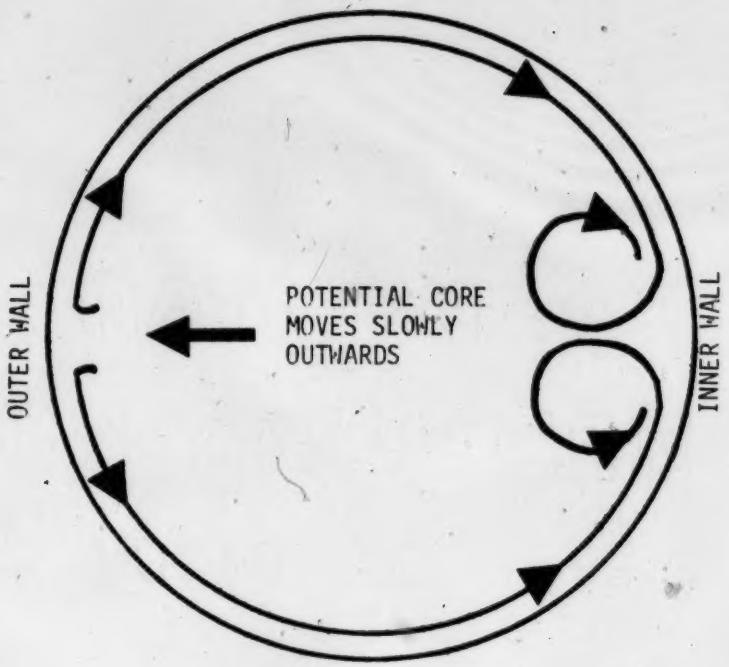

Figure 8.7 Trapped inner wall vortices

a.

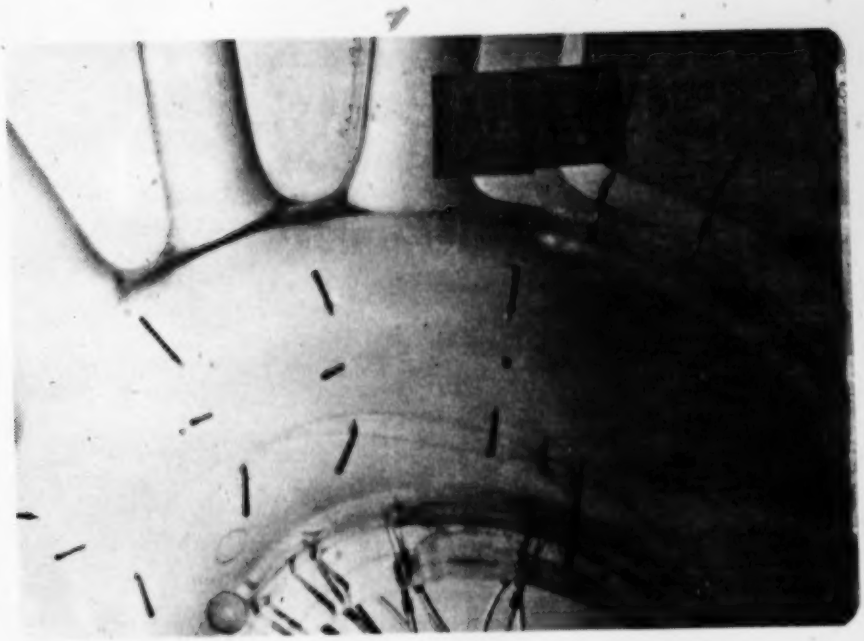

b.

Figure 8.8 Dye streams twisting in inner wall vortex

9. Conclusions

The major objective of this experiment, to determine whether or not a separation zone exists at the location of maximum curvature of the aortic arch, has been resolved. The separation zone can definitely be detected in steady flow when the Reynolds number exceeds 1000 and in pulsatile flow it persists throughout the cycle. The effect of the separation zone on disease development can be attributed to any one of the following: compressive stresses on the wall towards the separation line; fluctuating wall stress due to continuous movement of the separation line; and recirculation within the separation bubble inhibiting adequate scouring of the walls and transport of harmful elements away from the area.

Earlier results (Rodkiewicz,1975) demonstrating the correlation between separation locations and atherosclerosis predilection sites in the branches and along the outer curve wall, left the inner curve separation as the main point of contention. Although this separation was present in the open channel model (Rodkiewicz,1975) and was seen in a three-dimensional model,[1] no concrete evidence in the form of photographs was obtainable. Therefore a debate ensued, since Scarton et al.(1976) demonstrated that no separation occurred in a curved converging tube. His claim that the branches do not significantly affect the flow in the arch is unfounded, as borne out by the results of this experiment. The branches are in effect the sole factor determining the

[1] Dr.C.M.Rodkiewicz, Univ. of Alberta; personal communication

existence of the inner curve separation zone. The branches act as a diffuser, lowering the velocity in the arch in that area, thereby increasing the pressure and causing the adverse pressure gradient required for flow separation. Without the branches, a converging tube with the same curvature ratio as the arch does not show separation for the full physiological range of Reynolds number.

This study provides the final link in the hypothesis that each atherogenesis site in the arch corresponds to a separation or stagnation zone in the flow. The overwhelming evidence of this correlation should now provide a basis for further biochemical studies to determine the pathological mechanism of atherogenesis as it relates to stresses induced by the blood flow patterns.

References

Altman,P. and Dittmer,D. (1971) Respiration and Circulation Federation of American Societies for Experimental Biology. Maryland, U.S.

Atabek,H.B.,Chang,C.C. and Fingerson,L.M. (1964) Measurement of laminar oscillatory flow in the inlet length of a circular tube. Phys. in Med. Biology, Vol.9, pp.219-227.

Austin,L.R. and Seader,J.D. (1973) Fully developed viscous flow in coiled circular pipes. AICHE J. Vol.19, pp.85-94.

Bayliss,L.E. (1962) The rheology of blood. In 'Handbook of Physiology', Sec.2 (Circulation), Vol.1, ch.8. Washington: American Physiological Society.

Bergel,D.H. (1972) Cardiovascular Fluid Dynamics. Academic Press Inc., New York.

Best,C. and Taylor,N. (1952) The Living Body. Henry Holt and Company, New York.

Caro,C.G.,Fitz-Gerald,J.M. and Schroter,R.C. (1971) Atheroma and arterial wall shear; Observation, correlation and proposal of a shear dependant mass transfer mechanism for atherogenesis. Proc.Roy.Soc.Lond. B , Vol.177, pp.109-159.

Chandran,K.B.,Swanson,W.M.,Ghista,D.N. and Vayo,H.W. (1974) Oscillatory flow in thin-walled curved elastic tubes. Annals of Biomedical Eng., Vol.4, pp.392-412.

Chien,S. (1979) Blood Rheology. in Quantitative Cardiovascular Studies, ed. Hwang,N.,Gross,D.R. and Patel,D.J. University Park Press, Baltimore.

Dean,W.R. (1927) Note on the motion of fluid in a curved pipe. Phil.Mag., Vol.4, pp.208-223.

Detweiler,D.K. (1972) Circulation. W.B.Saunders Co., Philadelphia.

Dotter,C. and Steinberg,I. (1949) The angiocardiographic measurement of the normal great vessels. Radiology, Vol.52, pp.353-358.

Farthing,S.,Peronneau,P. (1979) Flow in the thoracic aorta. Cardiovasc. Res., Vol.XIII, pp.607-620.

Franklin,D.L.,Ellis,R.M. and Rushmer,R.F. (1959) Aortic blood flow in dogs during treadmill exercise. J.Appl.Physiol., Vol.14, pp.809-812.

Franklin,D.L.,Schlegel,W. and Rushmer,R.F. (1961) Blood flow measured by Doppler frequency shift back-scattered sound. Science, Vol.134, pp.564-565.

Fry,D.L. (1968) Acute vascular endothelial changes associated with increased blood velocity gradients. Circulation Research, Vol.XXII, pp.165-197.

Furukawa,K.,Yoshikawa,J.,Tanaka,K.,Tanaka,C.,Kawai,S., Takeuchi,K. and Shiota,K. (1976) Echocardiographic measurement of aortic root diameter. Japanese Heart Journal, Vol.17, pp.465-470.

Gabe,I.T.,Gault,J.H.,Ross,J.Jr.,Mason,D.T.,Mills,C.J., Shillingford,J.P. and Braunwald,E. (1969) Measurement of instantaneous blood flow velocity and pressure in conscious man with a catheter-tip velocity probe. Circulation, Vol.40, pp.603-614.

Grant,B. (1951) An Atlas of Anatomy. The Williams and Wilkins Co., Baltimore.

Gray,P. and Elliot,A. (1943) The specific gravity of whole blood and serum. Amer.J. of Med.Sciences, Vol.205, pp.356.

Gresham,G.A. (1976) Primate Atherosclerosis. S.Karger-Basel, New York.

Guyton,A.C. (1956) Textbook of Medical Physiology. W.B.Saunders Co., Philadelphia.

Haynes,R.H. (1961) The rheology of blood. Trans. Soc. Rheol., Vol.5, pp.85-101.

Hildebrandt,J. (1981) Finite element modelling of fluid motion and damped acoustic waves in pipes. M.Sc. thesis, Univ. of Alberta.

Kolin,A. (1936) An electromagnetic flowmeter. Principle of the method and its application to blood flow measurements. Proc.Soc.Exp.Biol.Med., Vol.35, pp.53-56.

Kolin,A. (1937) An electromagnetic recording flowmeter. Amer.J.Physiol., Vol.119, p.355.

Ling,S.C.,Atabek,H.B.,Fry,D.L.,Patel,D.J. and Janicki,J.S. (1968) Application of heated-film velocity and shear probes to hemodynamic studies. Circulation research, Vol.23, pp.789-801.

Machella,T.E. (1936) The velocity of blood flow in arteries in animals. Amer.J.Physiol., Vol.115, pp.632-644.

McDonald,D. (1974) Blood Flow in Arteries. Edward Arnold Ltd., London.

Meschan,I. (1975) An Atlas of Anatomy Basic to Radiology. W.B.Saunders Co., Philadelphia.

Miller,D.S. (1971) Internal Flow. A Guide to Losses in Pipe and Duct Systems. The British Hydromechanics Research Association, Cranfield,Bedford,England.

Mills,C.J. (1966) A catheter-tip electromagnetic velocity probe. Phys. in Med. Biol., Vol.11, pp.323-324.

Mills,C.J. and Shillingford,J.P. (1967) A catheter-tip electromagnetic velocity probe and its evaluation. Cardiovascular Res., Vol.1, pp.263-273.

Mills,C.J.,Gabe,I.T.,Gault,J.H.,Mason,D.T.,Ross,J., Braunwald,E. and Shillingford,J.P. (1970) Pressure-flow relationships and vascular impedance in man. Cardiovasc.Res., Vol.4, pp.405-417.

Muirhead,E.,Grow,M. and Walker,A. (1946) Practical observations on the copper sulphate method for determining the specific gravities of whole blood and serum. Surgery,Gynecology and Obstetrics, Vol.82, pp.405-413.

Nichols,W.W.,Conti,C.R.,Walker,W.E. and Milnor,W.R. (1977a) Input impedance of the systemic circulation in man. Circulation Res., Vol.40, pp.451-458.

Nichols,W.W.,Conti,C.R. and Pepine,C.J. (1977b) Instantaneous force-velocity-length relations in the intact human heart. The American Journal of Cardiology, Vol.40, p.756.

Prec,O.,Katz,L.N.,Sennett,L.,Roseman,R.H.,Fishman,A.P. and Hwang,W. (1949) Determination of the kinetic energy in the heart of man. Amer.J.Physiol., Vol.159, pp.483-491.

Reich,N.E. (1949) Diseases of the Aorta. Diagnosis and Treatment. The Macmillan Co., New York.

Reul,H.,Tesch,B.,Schoenmackers,J. and Effert,S. (1974) A hydromechanic model of left ventrical, aorta and its branches. Simulation of geometry,haemodynamics and elasticity. Basic Res. in Cardiology, Vol.69, No.3, pp.257-265.

Rodkiewicz,C.M. and Roussel,C.L. (1973) Fluid mechanics in a large arterial bifurcation, Trans. ASME, J. of Fluids Eng., Vol 95, Series I, pp.108-112.

Rodkiewicz,C.M. (1975) Localization of early atherosclerotic lesions in the aortic arch in the light of fluid flow. J. of Biomechanics,Vol 8,No.2, pp.149-156.

Rodkiewicz,C.M.,Kuchar,N.R. and Behan,S. (1976a) Flow characteristics of the aortic arch. U. of Alberta Report No.3.

Rodkiewicz,C.M. (1976b) On the transport in large arteries. U. of Alberta Report No.21.

Rodkiewicz,C.M. and Hung,R. (1976c) Flow division dependance of some large arterial junctions on frequency and

amplitude. U. of Alberta Report No.5

Rodkiewicz,C.M. and Kalita,W. (1978) Flow characteristics of curved pipe junctions, Departmental Report No.12, Univ. of Alberta, Edmonton.

Rodkiewicz,C.M.,Zajac,S.,Jadruch,W.T. and Hsieh,W. (1979) Effect of aortic arch atherosclerotic formations on blood mass flow distribution. J. of Biomed. Eng., Vol.101, pp.96-104.

Rosenblatt,G.,Stokes,J.III and Bassett,D. (1965) Whole blood viscosity, hematocrit, and serum lipid levels in normal subjects and patients with coronary heart disease. J. Lab. and Clinical Med., Vol.65, pp.202-211.

Roussel,C.L. (1971) Flow Characteritics in Arterial Junctions. M.Sc. thesis, Univ. of Alberta.

Ruch,T. and Patton,H. (1973) Physiology and Biophysics II. Circulation, Respiration and Fluid Balance. W.B.Saunders Co., Philadelphia.

Rushmer,R.D. (1970) Cardiovascular Dynamics. W.B.Saunders Co., Toronto.

Scarton,H.A., Shah,P.M., Tsapogas,M.J., (1976) Relationship of the spacial evolution of secondary flow in curved tubes to the aortic arch.(unpublished)

Schlichting,H. (1968) Boundary-Layer Theory. McGraw-Hill, New York.

Seed,W.A. and Wood,N.B. (1970) Development and evaluation of a hot-film velocity probe for cardiovascular studies. Cardiovascular Research, Vol.4, pp.253-263.

Seed,W.A. and Wood,N.B. (1971) Velocity patterns in the aorta. Cardiovascular Research, Vol.5, pp.319-330.

Shah,P.,Scarton,H.,Tsapogas,M. and Balasubramaniam,N. (1976) Study on the hemodynamics in a simulated aortic arch and its possible effects on atherosclerosis. Proceedings of

the Twentieth World Congress of the International College of Surgeons. Athens,Greece.

Singh,M.P. (1974) Entry flow in a curved pipe. J.Fluid Mechanics, Vol.65, part 3, pp.517-539.

Smith,F.T., (1975) Pulsatile flow in curved pipes. J.Fl.Mech.,Vol.71,pt.1, pp.15-42.

Timm,C. (1942) Der Stromungsverlauf in einem Modeli der menschlichen Aorta. Zeitschrift fur Biologie, Vol.121, pp.79-99.

Uchida,Shigeo, (1956) The pulsating viscous flow superposed on the steady laminar motion of incompressible fluid in a circular pipe. ZAMP,Vol. VII, pp.403-422.

White,C.M. (1929) Streamline flow through curved pipes. Proc.Roy.Soc.London A., Vol.123, pp.645.

Womersley,J.R. (1955a) Oscillatory motion of a viscous liquid in a thin-walled elastic tube. I. The linear approximation for long waves. Phil.Mag., Vol.46, pp.199-221.

Womersley,J.R., (1955b) Method for the calculation of velocity, rate of flow and viscous drag in arteries when the pressure gradient is known. J. Physiology, Vol.127, pp.553-563.

Appendix I : Glossary

atheroma: a condition marked by the depositing of small fatty nodules on the inner walls of the arteries, and by degeneration of the affected areas; also such a nodule

arteriosclerosis: a thickening and loss of elasticity of the walls of the arteries

atherogenesis: the primary stage of atherosclerosis

atherosclerosis: a thickening of and loss of elasticity in the inner walls of arteries, accompanied by the formation of atheromas

atrium: a chamber of the heart which receives blood from the veins and pumps it into the corresponding ventricle

average: a weighing with respect to spatial coordinates

brachiocephalic: a main artery originating at the aortic arch, which splits into the right subclavian and right common carotid artery

carotid: the principal artery of the neck, leading to the brain

coronary artery: artery feeding blood to the heart muscle

diastole: the stage of dilation of the ventricles

hematocrit: a ratio of volume of packed red blood cells to volume of whole blood

intracardiac: existing or occurring within the heart

intravascular: situated or occurring within a blood vessel

in vivo: in the living body of an animal (including humans)

lumen: the cavity of a tubular organ

mean: a weighing with respect to time

plasma: the fluid part of blood as distinguished from suspended material

proximal: next to or nearest the point of attachment or origin or point of view

sclerosis: an abnormal hardening of the walls of arteries

sinus of Vasalva: a dilation of the aorta at the level of the coronary arteries

subclavian: the proximal part of the main artery of the arm or forelimb

systole: the contraction of the heart by which the blood is forced onward

ventricle: a chamber of the heart which receives blood from a corresponding atrium and from which blood is forced into the arteries

Appendix II : Non-dimensional parameters

The purpose of this section is to derive the parameters describing flow in a tube under pulsatile conditions. The constraints are that the tube is straight, rigid and circular. Under these conditions, the flow governing equation is given by:

$$\frac{\partial v}{\partial t} = \frac{-1}{\rho}\frac{\partial p}{\partial z} + \nu\left(\frac{\partial^2 v}{\partial r^2} + \frac{1}{r}\frac{\partial v}{\partial r}\right) \qquad \text{(II.1)}$$

where z is the axial coordinate. The coordinates, velocity components and pressure term are non-dimensionalized by use of the following transformations:

$$\begin{aligned} r &= Rr^+ & z &= Lz^+ \\ v &= \bar{v}v^+ & t &= \frac{1}{\omega}t^+ \\ p &= (\rho\bar{v}^2)p^+ \end{aligned} \qquad \text{(II.2)}$$

where the superscript plus denotes non-dimensional quantities and L is some arbitrary axial length.

Introducing these quantities into equation II.1 produces the following expression after rearranging:

$$\left[\frac{R^2\omega}{\nu}\right]\left[\frac{\nu}{\bar{v}R}\right]\frac{\partial v}{\partial t} = -\left[\frac{R}{L}\right]\frac{\partial p}{\partial z} + \left[\frac{\nu}{\bar{v}R}\right]\left\{\frac{\partial^2 v}{\partial r^2} + \frac{1}{r}\frac{\partial v}{\partial r}\right\} \qquad \text{(II.3)}$$

From equation II.3 it is possible to deduce the following set of non-dimensional parameters:

a. Length ratio: $Le = \frac{L}{R}$

b. Reynolds number: $Re = \frac{\bar{v}D}{\nu} = \frac{2\bar{v}R}{\nu}$ (II.4)

c. Frequency parameter: $\alpha = R\sqrt{\frac{\omega}{\nu}}$

Substituting II.4 into II.3 yields:

$$\frac{2\alpha^2}{Re}\frac{\partial v}{\partial t} = -\frac{1}{Le}\frac{\partial p}{\partial z} + \frac{2}{Re}\left[\frac{\partial^2 v}{\partial r^2} + \frac{1}{r}\frac{\partial v}{\partial r}\right] \qquad (II.5)$$

It is customary to adopt the definition of α given in equation II.4 (even though it produces the parameter squared in II.5) since α shows up again in the solution to equation II.1.

Equation II.5 can be applied to the case of pulsatile flow with zero net flowrate where the amplitude of the velocity wave is governed by the amplitude and frequency of the forcing function $\frac{dp}{dt}$. In a more realistic application for blood flow studies the forcing function consists of a constant pressure gradient term superimposed by a fluctuating component. This produces a net flowrate component and an oscillating flow component. The relative amplitudes of these components can be represented by a non-dimensional amplitude parameter (Kuchar and Scala, 1968):

$$\lambda = \frac{v_{max} - v_{min}}{\bar{v}} \qquad (II.6)$$

where λ represents the ratio of peak to peak velocity to

the steady velocity component. Of course if $v_{min}=0$ then becomes:

$$\lambda = \frac{v'}{\bar{v}} \qquad \text{(II.7)}$$

Heretofore, λ has primarily been used in applying a sinusoidal pulsation but is equally valid in scaling an actual pulsation to model proportions. In other words, to simulate an actual pulsation with a cam and piston arrangement requires input of the waveform to the design program but scaling can still be performed with the aid of the amplitude parameter.

The dimensionless length parameter is satisfied by reproducing the actual geometric ratios in the model. The Reynolds number is based on the mean inlet velocity which of course depends on the cardiac output so a representative value has been selected. Finally the frequency parameter $\alpha=19$ as an experimental choice is based on a heart rate of 70 beats/minute.

Appendix III : Cam Design

It is difficult to produce a feasible cam which would adequately simulate the heart pulsations. Therefore, the cams used in this experiment were designed through a versatile computer program. The program actually consists of two distinct subprograms. One subroutine was specifically designed for this experiment to generate a displacement curve from a representative velocity waveform of flow in the aorta. This displacement curve is then inputted to the cam design subroutine. The second subroutine produces the profile of a disk cam with reciprocating follower from input data of the corresponding displacement curve. This routine is very general and accepts a wide range of input parameters.

The input to the displacement subroutine is a series of data points from an average velocity vs time trace of flow in an actual aorta. To reproduce a similar waveform in the model, the scaling of the velocity curve must be modified so that the non-dimensional parameters α and Re are both satisfied.

The vertical scale is determined by the Reynolds number:

$$\frac{v_1 D_1}{\nu_1} = \frac{v_2 D_2}{\nu_2}$$

$$\therefore \frac{v_1}{v_2} = \left(\frac{D_2}{D_1}\right)\left(\frac{\nu_1}{\nu_2}\right) \qquad \text{(III.1)}$$

where subscripts 1 and 2 refer to model and aorta respectively. Since the cam superimposes a fluctuation over the steady flow from the pump, this must be accounted for by subtracting the steady velocity component from the instantaneous velocity:

$$v = v_1 - \frac{1}{T} \int_0^T v_1(t)dt \qquad \text{(III.2)}$$

Finally, the vertical scale of the velocity curve is adjusted to allow for the difference between the piston bore and the diameter of the model inlet.

The horizontal or time scale must be determined from the period of the fluctuation which is inversely proportional to the frequency. The frequency of the flow in the model must be set to satisfy α:

$$R_1\sqrt{\frac{\omega_1}{\nu_1}} = R_2\sqrt{\frac{\omega_2}{\nu_2}}$$

$$\therefore \frac{\omega_1}{\omega_2} = \left(\frac{R_2}{R_1}\right)^2 \frac{\nu_1}{\nu_2} \qquad \text{(III.3)}$$

Once the scaling is completed, the subprogram integrates the velocity curve by Simpson's rule to yield the corresponding displacement profile. It can be noted that the vertical scale is proportional to the viscosity ratio and the horizontal scale is inversely proportional to this ratio. Therefore, when integrating, the viscosity ratio term drops out of the equation. In other words, the cam profile

does not depend in any way on the working fluid being used in the model. The displacement curve corresponding to the velocity profile from Figure 4.6 is shown in Figure III.1.

The cam subroutine then reads in data points from the displacement curve, asks for a base circle radius and converts the horizontal scale to degrees of rotation, bringing the design to a stage where the pitch profile can be plotted. Due to the sudden increase in velocity at the beginning of systole, the pressure angle on a centered cam is much too high for the cam to be practicable. Therefore, the program was expanded to allow for offsetting the cam to reduce the pressure angle when required. Finally, using simple calculus, the program determines the inward normal to the pitch profile at each data point, marks off a distance along the normal equal to the follower radius (as specified by the programmer) and is thus in a position to plot the complete cam profile and quote the maximum pressure angle for the given design. The pitch and cam profiles corresponding to the waveform in an actual aorta are shown in Figure III.2.

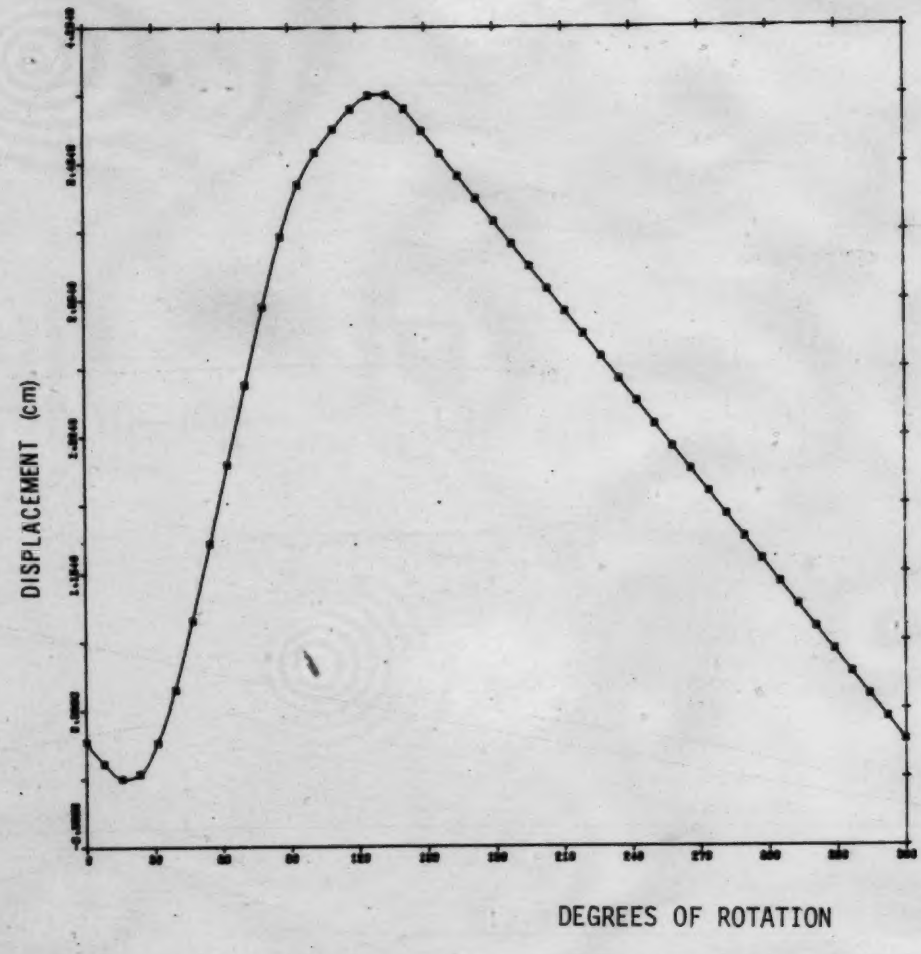

Figure III.1 Displacement curve

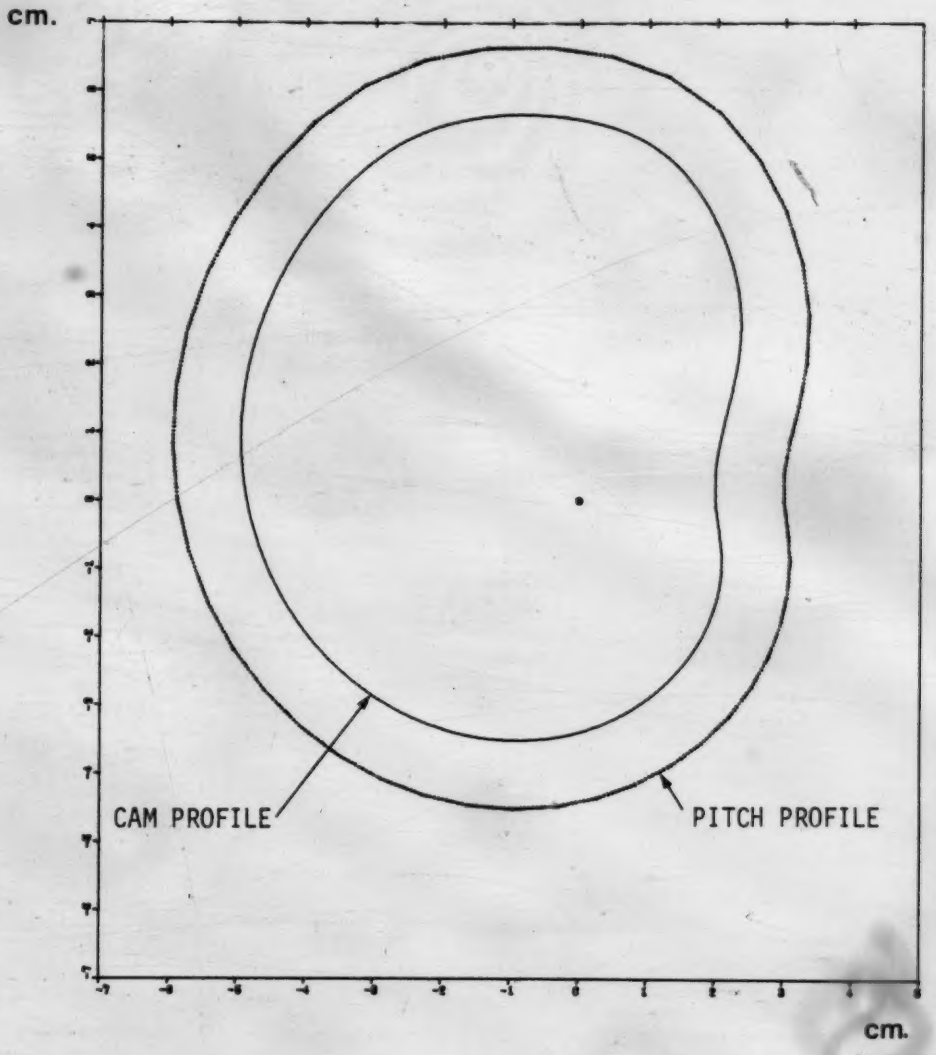

Figure III.2 Cam and pitch profiles

Appendix IV : Injection Points

The locations of the dye injection points must be accurately specified so that flow characteristics displayed at various locations can be integrated into a single complete flow pattern. Since the model is three times actual size, it is advantageous to use a non-dimensionalized coordinate system to denote the infusion sites. Two coordinates S and θ, are used where:

S = distance along the centreline of the aortic arch from the inlet plane

θ = angle (in radians) between a line OP normal to the centreline and passing through the injection point, and line OH which is the outward normal to S along the horizontal plane of symmetry (Fig.IV.1)

The downstream position is then non-dimensionalized by dividing by the inlet diameter of the arch D. Figure IV.2 indicates the numbering scheme for the wall taps and Table IV.1 presents the coordinates of each wall injection point. The tip of the inlet dye pipe is located at S=0.5cm. or S/D=0.06.

Table IV.1. Dye Tap Locations

Tap Number	S(cm)	S/D	θ(rads)
1	16.8	2.00	0.
2	16.8	2.00	1.57
3	18.3	2.18	0.
4	19.4	2.31	0.
5	21.1	2.51	0.
6	22.1	2.63	0.
7	22.5	2.68	1.28
8	22.5	2.68	1.57
9	22.5	2.68	1.86
10	22.5	2.68	3.14
11	26.9	3.20	1.25
12	26.9	3.20	1.57
13	26.9	3.20	1.89
14	26.9	3.20	3.14
15	30.1	3.58	1.25
16	30.1	3.58	1.57
17	30.1	3.58	1.89
18	33.8	4.02	1.28
19	33.8	4.02	1.57
20	33.8	4.02	1.84
21	35.4	4.21	0.
22	36.5	4.35	2.03
23	35.6	4.24	3.60
24	36.5	4.35	0.
25	40.7	4.85	0.
26	45.0	5.36	0.
27	9.5	1.13	2.76
28	9.5	1.13	3.14
29	9.5	1.13	3.52
30	13.5	1.61	2.76
31	13.5	1.61	3.14
32	13.5	1.61	3.52
33	22.5	2.68	2.83
34	22.5	2.68	3.46
35	26.9	3.20	2.83
36	26.9	3.20	3.46
37	30.1	3.58	2.83
38	30.1	3.58	3.14
39	30.1	3.58	3.46
40	36.5	4.35	2.83
41	36.5	4.35	3.14
42	36.5	4.35	3.46
43	31.9	3.80	2.83
44	31.9	3.80	3.14
45	31.9	3.80	3.46

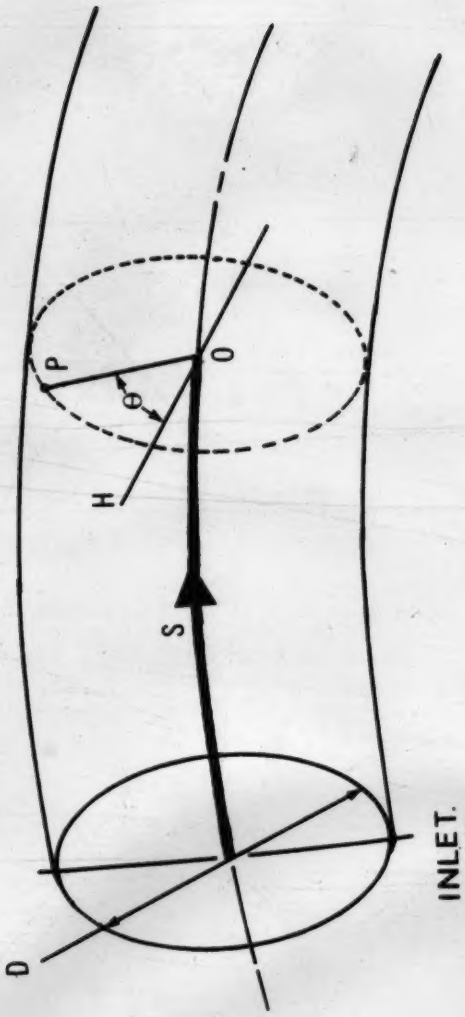

Figure IV.1. Coordinate System in Arch

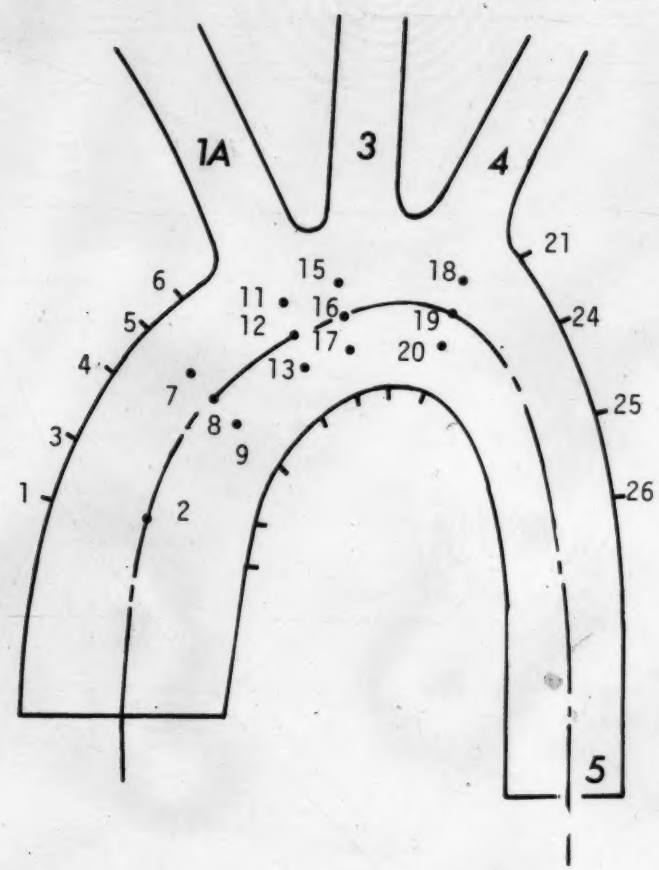

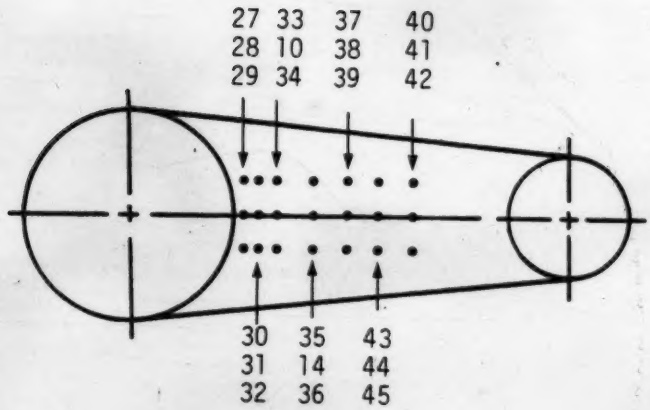

Figure IV.2 Dye pipe numbering

Appendix V : Inlet Section Design

As the velocity profile at the entrance to the aortic arch plays such a dominant role in the development of downstream flow patterns, it is imperative that the inlet section provide a means for complete momentum transfer across the channel. This is achieved by a series of polyester screens spaced evenly along the entrance pipe. The polyester material is precision woven and inert in water, therefore ideal for this application. The relevant criteria used to determine the appropriate mesh size and screen placement are:

a. the porosity of the screen should be about 50% and a range of 40-60% is acceptable, where porosity is defined as:

$$\beta = (1 - \frac{d}{W})^2 \qquad (V.1)$$

where d and W are the wire diameter and spacing respectively;

b. the screens should be placed at least 200 wire diameters apart, with about 1000 wire diameters after the final screen;

c. four screens should provide adequate transfer of momentum.

These rules of thumb are commonly used in experimental

practice[2] and have proven suitable in a wide range of applications. The first stipulation follows from the fact that a large porosity will not effectively transfer momentum, and a low porosity will cause a large pressure drop and unacceptable jetting effects. The second empirical condition allows enough space for the small scale eddies to damp somewhat before the following screen and the final spacing is recommended to completely dissipate any turbulence caused by the mesh. However, since it is also desirable to inhibit boundary layer growth upstream of the arch inlet, a compromise of 400 wire diameters after the last screen was settled upon. Finally, the additional mixing achieved by using more than four screens is usually not justified for the extra space and pressure drop required.

To satisfy these requirements, a screen with a thread diameter of 0.018 inches and mesh count/inch=21x21 was selected. This gives a porosity of ≈56% and an axial spacing of ≈2.4 inches. between screens.

---

[2]Dr.D.Wilson, Univ. of Alberta; personal communication